IRRADIATION EFFECTS ON REACTOR STRUCTURAL MATERIALS

L. E. Steele

Naval Research Laboratory
Washington, D. C.

15 November 1972

NRL Memorandum Report 2531

Irradiation Effects on Reactor Structural Materials

Quarterly Progresss Report 1 August - 31 October 1972

L. E. STEELE
Editor

Reactor Materials Branch
Metallurgy Division

November 15, 1972

NAVAL RESEARCH LABORATORY
Washington, D.C.

UNCLASSIFIED
Security Classification

DOCUMENT CONTROL DATA - R & D

(Security classification of title, body of abstract and indexing annotation must be entered when the overall report is classified)

1 ORIGINATING ACTIVITY *(Corporate author)*

Naval Research Laboratory
Washington, D. C. 20390

2a. REPORT SECURITY CLASSIFICATION

UNCLASSIFIED

2b. GROUP

---

3 REPORT TITLE

IRRADIATION EFFECTS ON REACTOR STRUCTURAL MATERIALS, QUARTERLY PROGRESS REPORT, 1 AUGUST - 31 OCTOBER 1972

4 DESCRIPTIVE NOTES *(Type of report and inclusive dates)*

This is a quarterly report of progress; work on these problems is continuing.

5 AUTHOR(S) *(First name, middle initial, last name)*

Steele, L. E., editor

6 REPORT DATE	7a. TOTAL NO. OF PAGES	7b. NO. OF REFS
November 15, 1972	51	16

8a. CONTRACT OR GRANT NO

NRL Problems M01-14, M01-22, M01-27

b. PROJECT NO

RR022-11-41-5409, RR022-11-41-5425,

c. RR022-11-41-5426

AEC-AT(49-5)-2110

d. MIPR-ERG-41004

9a. ORIGINATOR'S REPORT NUMBER(S)

NRL Memorandum Report 2531

9b. OTHER REPORT NO(S) *(Any other numbers that may be assigned this report)*

10 DISTRIBUTION STATEMENT

Approved for public release; distribution unlimited.

11. SUPPLEMENTARY NOTES

Also sponsored by:
U.S. Atomic Energy Commission
DRDT, Washington, D.C. 20545

12 SPONSORING MILITARY ACTIVITY

Dept.of the Navy (Office of Naval Research), Washington, D.C., and Dept. of the Army (Army Nuclear Power Program), Ft.Belvoir, Va.

13 ABSTRACT

The research program of the NRL Metallurgy Division, Reactor Materials Branch, involves a broad study of the effects of nuclear radiation upon materials. The program is sponsored by the Office of Naval Research, the U. S. Atomic Energy Commission, and the Army Nuclear Power Program. Since research findings which apply to the objectives of one sponsoring agency are also of interest to the others, the overall program progress is reported herein. This report, covering research for the period 1 August-31 October 1972, includes: (1) J-integral characterization of irradiated 304 stainless steel, (2) studies of fatigue crack propagation in neutron irradiated stainless steel weldments, (3) exploratory assessments of A508 forging radiation resistance, (4) a parametric study of the vacancy trapping during irradiation, and (5) surveillance results for the MH-1A reactor pressure vessel.

DD FORM 1 NOV 65 1473 (PAGE 1)

S/N 0102-014-6600

UNCLASSIFIED
Security Classification

14 KEY WORDS	LINK A		LINK B		LINK C	
	ROLE	WT	ROLE	WT	ROLE	WT
Dislocation loops						
Displacements						
Elastic plastic fracture						
Electron microscopy						
Fatigue crack growth						
Fatigue crack initiation						
Fracture						
Helium particles						
J -integral						
MH-1A reactor						
Neutron radiation - reactors						
Pressure vessel steel						
Ratio Analysis Diagram (RAD)						
Radiation damage						
Radiation damage mechanisms						
Stainless steel						
Shelf energy						
Stress intensity factor						
Surveillance						
Vacancies						
Vacancy trapping						
Void nucleation						

PREFACE

This report represents, collectively, the progress for the quarter, 1 August - 31 October 1972, by various members of the Metallurgy Division, Reactor Materials Branch. These include, in order of the appearance of their work:

F. J. Loss
R. A. Gray, Jr.
P. Shahinian
H. E. Watson
H. H. Smith
J. R. Hawthorne
F. A. Smidt, Jr.
J. A. Sprague
C. Z. Serpan, Jr.

Individual credit is given with each report section heading.

CONTENTS

IRRADIATION EFFECTS ON REACTOR STRUCTURAL MATERIALS
QUARTERLY PROGRESS REPORT
1 August - 31 October 1972

SUMMARY

I. ADVANCED REACTOR MATERIALS

A. J-Integral Characterization of Irradiated Stainless Steels

The J integral is being investigated as a method to characterize the elastic plastic toughness level of structural materials used in advanced fast reactors. J values are presented for irradiated 304 stainless steel in the annealed and cold worked conditions and for 308 stainless steel weld metal; approximate methods for J-integral calculations are described and also applied to specimen evaluations. Results indicate the cold worked material to exhibit a significantly lower toughness than the annealed material in both irradiated and unirradiated conditions. Radiation significantly degrades the toughness of the annealed material while showing relatively little effect on the cold worked specimens. J evaluations of unirradiated, annealed stainless steel at room temperature and 1000°F (538°C) indicate that elevated temperature markedly lowers the J values based on conditions at maximum load on the specimen. The toughness of the unirradiated weld metal is significantly less than that of the unirradiated plate. Flow properties, using rectangular compression specimens, are presented in support of the J-integral determinations.

B. Fatigue Crack Propagation in Neutron Irradiated Stainless Steel Weldments

The resistance to fatigue crack propagation of EBR-II irradiated Types 308 and 316 weld metals have been evaluated at 800 and 1100°F (427 and 593°C). Rates of crack growth were determined as a function of the stress intensity factor range. In general, the crack propagation resistance was slightly lower for the irradiated metal than the unirradiated weld metal for both steels.

IRRADIATION EFFECTS ON REACTOR STRUCTURAL MATERIALS
QUARTERLY PROGRESS REPORT
1 August - 31 October 1972

SUMMARY

I. ADVANCED REACTOR MATERIALS

A. J-Integral Characterization of Irradiated Stainless Steels

The J integral is being investigated as a method to characterize the elastic plastic toughness level of structural materials used in advanced fast reactors. J values are presented for irradiated 304 stainless steel in the annealed and cold worked conditions and for 308 stainless steel weld metal; approximate methods for J-integral calculations are described and also applied to specimen evaluations. Results indicate the cold worked material to exhibit a significantly lower toughness than the annealed material in both irradiated and unirradiated conditions. Radiation significantly degrades the toughness of the annealed material while showing relatively little effect on the cold worked specimens. J evaluations of unirradiated, annealed stainless steel at room temperature and 1000°F (538°C) indicate that elevated temperature markedly lowers the J values based on conditions at maximum load on the specimen. The toughness of the unirradiated weld metal is significantly less than that of the unirradiated plate. Flow properties, using rectangular compression specimens, are presented in support of the J-integral determinations.

B. Fatigue Crack Propagation in Neutron Irradiated Stainless Steel Weldments

The resistance to fatigue crack propagation of EBR-II irradiated Types 308 and 316 weld metals have been evaluated at 800 and 1100°F (427 and 593°C). Rates of crack growth were determined as a function of the stress intensity factor range. In general, the crack propagation resistance was slightly lower for the irradiated metal than the unirradiated weld metal for both steels.

C. Exploratory Assessments of A508 Forging Radiation Resistance

The radiation embrittlement resistance of A508 forgings has been explored with two A508-2 forgings (12-in. and 9-1/2 in. thick) and one A508-4 forging (23-1/2-in. thick).

Comparisons of preirradiation Charpy-V versus drop weight performance by the A508-2 forgings showed the Charpy-V energy level corresponding to NDT to vary significantly (44 ft-lb in one case but 100 ft-lb in the second case). Consequently, NDT temperatures for this type forging cannot be predicted reliably with an arbitrary Charpy-V "energy fix".

Significant variability in 550°F (288°C) radiation embrittlement resistance was also observed. The apparent resistance to radiation embrittlement of one forging (A508-2) was equal to the average resistance exhibited by A533-B plate and weld deposits; the radiation resistance of the remaining forgings was on par with the highest resistance found for A533-B plate and weld deposits from standard commercial production. Residual impurity differences are suspected of being responsible for the variation observed in irradiation response.

Limited assessments of postirradiation notch ductility recovery by 650°F (343°C) heat treatment revealed a significant potential for embrittlement relief by this method.

II. RADIATION DAMAGE MECHANISMS

A. A Parametric Study of the Vacancy Trapping During Irradiation

Impurities have been found to influence the defect microstructure in Fe-.3Cu alloys irradiated at 280°C (535°F) to a fluence of 8.0×10^{20} n/cm^2 >0.1 MeV where loop nucleation is enhanced and in Fe-.3V alloys irradiated at 525°C (975°F) to a fluence of 8.5×10^{21} n/cm^2 >0.1 MeV where void formation is found to be suppressed. These results are considered in the light of a vacancy trapping mechanism. The vacancy concentration is found to be depressed and this in turn suppresses void and loop nucleation. It is concluded that the suppression of void formation in the Fe-V alloy can be explained by this theory but loop formation in the Fe-Cu alloy requires a heterogeneous nucleation mechanism which builds up through the trapped vacancies.

III. CURRENT REACTOR PRESSURE VESSEL STEELS

A. Pressure Vessel Surveillance of the MH-1A Reactor

A second accelerated-located surveillance capsule and vessel wall flux detector have been removed from the MH-1A reactor for analysis at NRL. Charpy specimens were V-notched in the hot cell and tested to show a reduction in upper shelf energy level closely matching previous results from the initial surveillance evaluation. Even at the highest fluence levels, an upper shelf level of about 150 ft-lb is retained. Tension test characteristics revealed rapid increases in yield strength and related degradation in reduction in area and elongation values. However, a high margin of ductility in tension remains. The neutron flux level for the peak flux plane was 1.1×10^{11} n/cm^2/sec >1 MeV, a lower value than originally measured. The flux at the vessel circumferential weld was 85 percent of this value. A 20-year full power fluence value of 6.9×10^{19} n/cm^2 >1 MeV was estimated for the reactor vessel.

RESEARCH PROGRESS

I. ADVANCED REACTOR MATERIALS

A. J-Integral Characterization of Irradiated Stainless Steels

F. J. Loss and R. A. Gray, Jr.

Introduction

The austenitic stainless steels used as structural materials in the LMFBR's are normally ductile in their virgin condition. However, environmental effects such as irradiation, high temperature and associated creep effects, and compatibility with the liquid sodium coolant can embrittle the steel so that its toughness is lowered from the fully plastic regime to the elastic plastic regime, and fracture becomes a consideration. Analytical description of the critical flaw size/stress level interaction has been highly developed for materials whose toughness falls into the linear elastic or brittle area, i.e., linear elastic fracture mechanics. However, a similar characterization for elastic plastic materials is exceedingly difficult because the material behaves in a nonlinear fashion due to the plasticity in the vicinity of the flaw. Several advanced procedures are being considered to analyze the elastic plastic regime. Of these, the J integral appears to offer the most attractive possibilities for a near term engineering solution in this area.

As described in Reference 1, the J integral is a mathematical concept that characterizes the average displacement field in the crack-tip vicinity and it can be related to a critical flaw size/stress level. This formulation is readily expressed in terms of loads and deflections at the boundaries of the specimen or structure, thereby providing a simple, straightforward evaluation technique. A research program has been undertaken to define the applicability of the J integral concept to structural materials used in advanced fast reactors.

The initial program effort consists of irradiation, in the EBR-II and ATR reactors, of notched, 3-point bend specimens of various geometries. Materials irradiated to date are 304 and 316 stainless steel (SS) plate in the annealed and cold worked (CW) conditions, including shielded metal arc (SMA) and submerged arc (S/A) welds of these steels, and Inconel 718. Experimental evaluation procedures require obtaining load vs deflection records from a test specimen and determining the conditions under which the crack front extends either by slow stable tearing or by an instability condition that leads to rapid crack extension. These

records may be evaluated by any of several techniques as described below.

In support of the J evaluations, flow properties are being obtained for each representative irradiation and testing condition. These properties are used in determining the specimen plastic zone sizes and in the calculation of plastic limit load conditions. Instability strains are being investigated as a fundamental material property with which to further describe the fracture process on a local scale and then to correlate with the overall specimen behavior.

Flow Properties of Irradiated Stainless Steels

The compressive properties of 304 SS irradiated and unirradiated, in both CW and CW plus annealed conditions, have been evaluated as a function of temperature. Two sections of a 1-in. thick plate of reactor grade 304 SS were cold rolled to a 25% reduction in thickness. Part of this material was then solution annealed at 1900°F (1038°C) for 30 minutes. Compression specimens were removed from the plates at the surface and one-half thickness (1/2T) locations in the longitudinal (LS) and transverse (SL) orientations.* A selected group of these specimens was irradiated in the Advanced Test Reactor to a fluence of 1.08×10^{21} n/cm^2 >0.1 MeV at 530°F (278°C). The results of this test program are summarized in Figs. 1 to 4. The specimens, simple rectangular prismatic bars (0.197-in. square by 0.433-in. long), were compressed between rigid parallel anvils and the transmitted load and specimen deflection were recorded. The testing was accomplished at a strain rate of less than 2×10^{-4} sec^{-1}.

The critical strain or work hardening coefficient, n, and ultimate tensile strength (UTS) were found in each case using the Considère construction technique[2]. This technique requires the use of true stress and engineering tensile strain values. In converting the compression data to these values, an adjustment must be applied to the longitudinal strain to accommodate the end effects (i.e., the specimens takes on a "barrel shape" after loading). A method of determining this barreling correction has been evolved by Krafft[3] based on the assumption that the areal strain at the axial midlength of the compression specimen is the least affected by frictional constraint at the end surfaces and is indicative of the behavior of material unaffected by end conditions. The empirically drived equation for the specimen geometry tested yields a corrected longitudinal engineering compressive strain (e_c):

*LS - specimen axis parallel to the rolling direction
SL - specimen axis perpendicular to the rolling direction, parallel to plate surface[4].

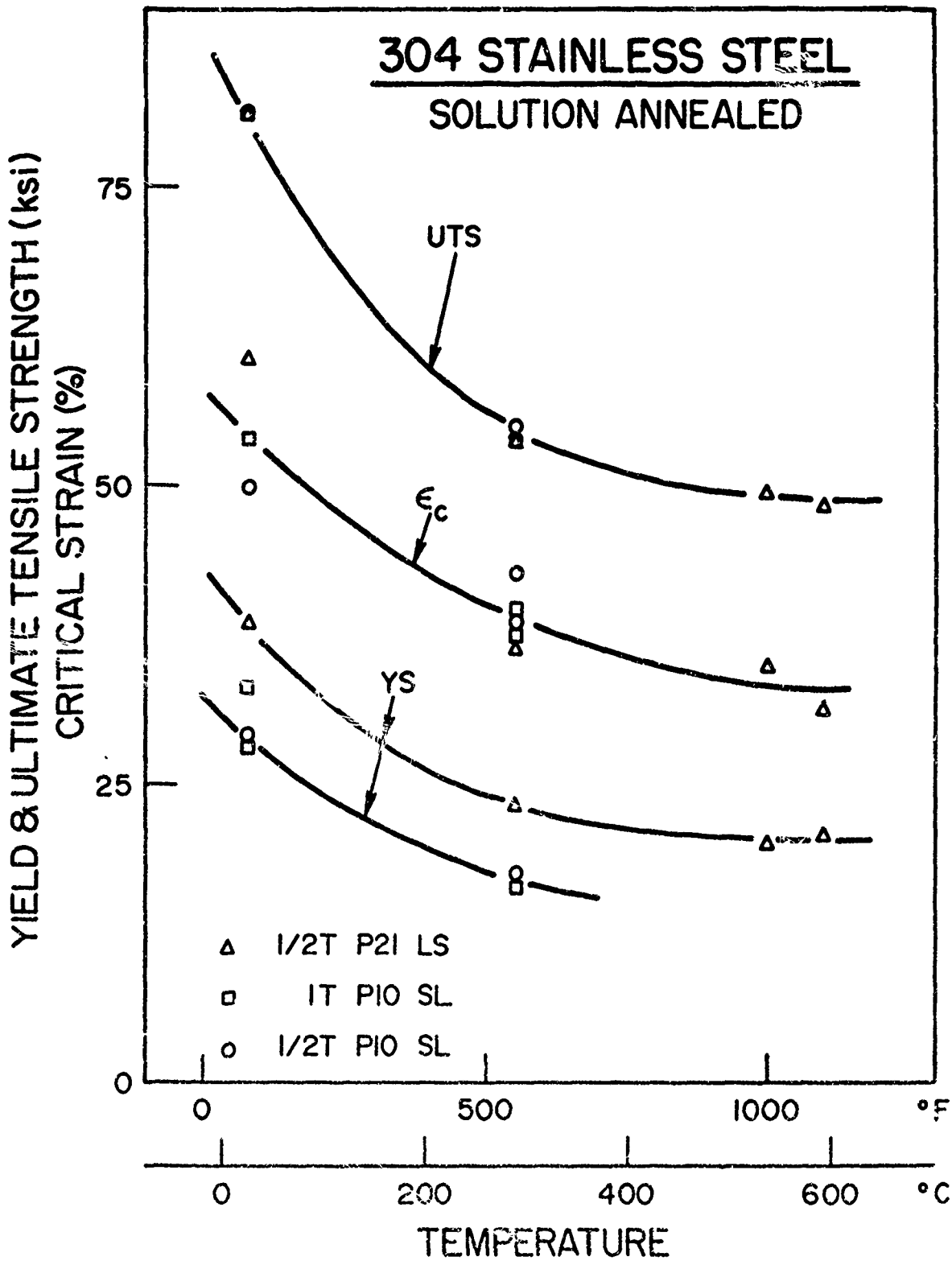

Fig. 1 - Ultimate tensile strength (UTS), yield strength (YS), and critical stain (ϵ_c) as a function of temperature for Type 304 stainless steel in the annealed condition.

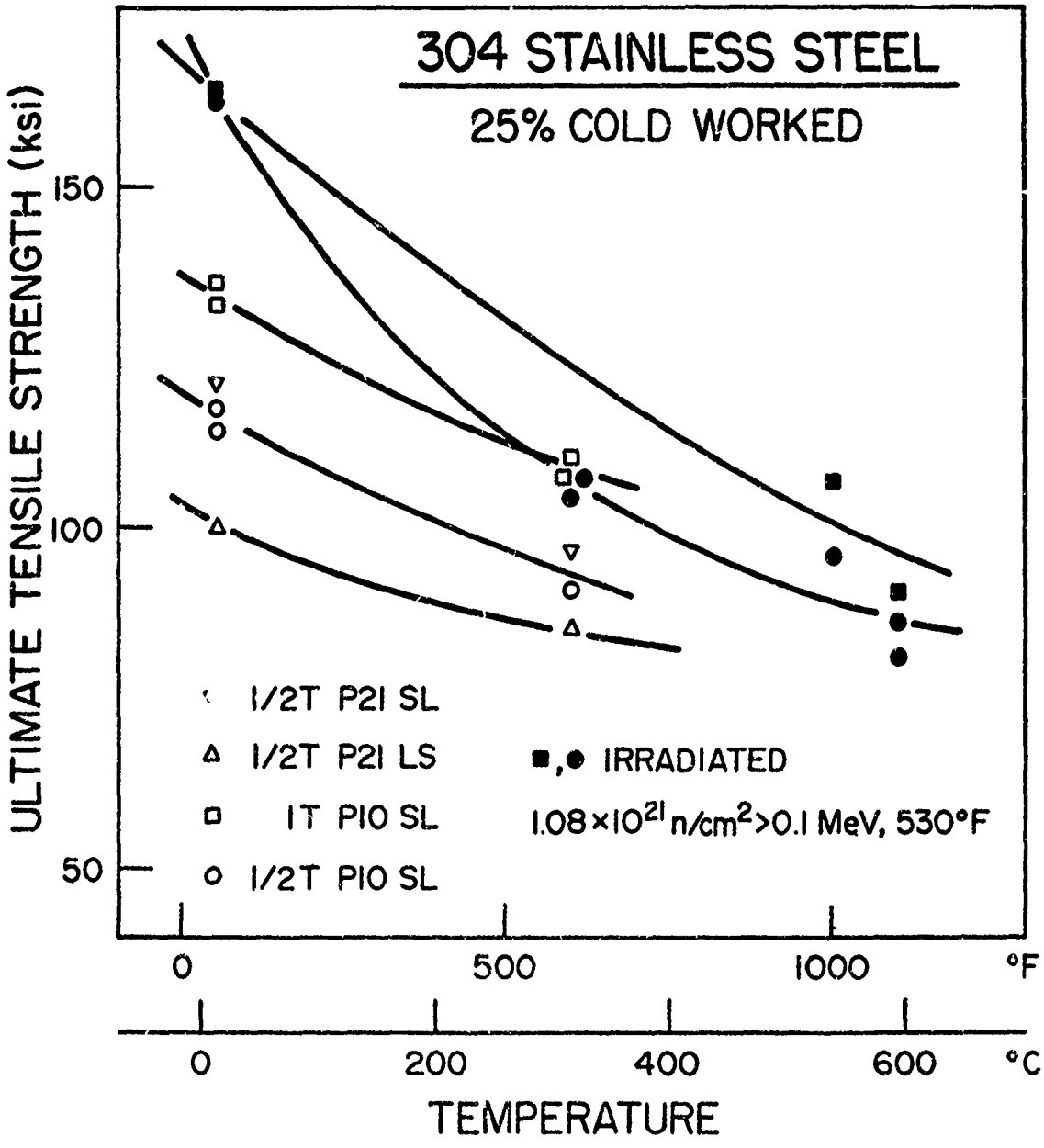

Fig. 2 - Yield strength as a function of temperature for 25% cold worked Type 304 stainless steel.

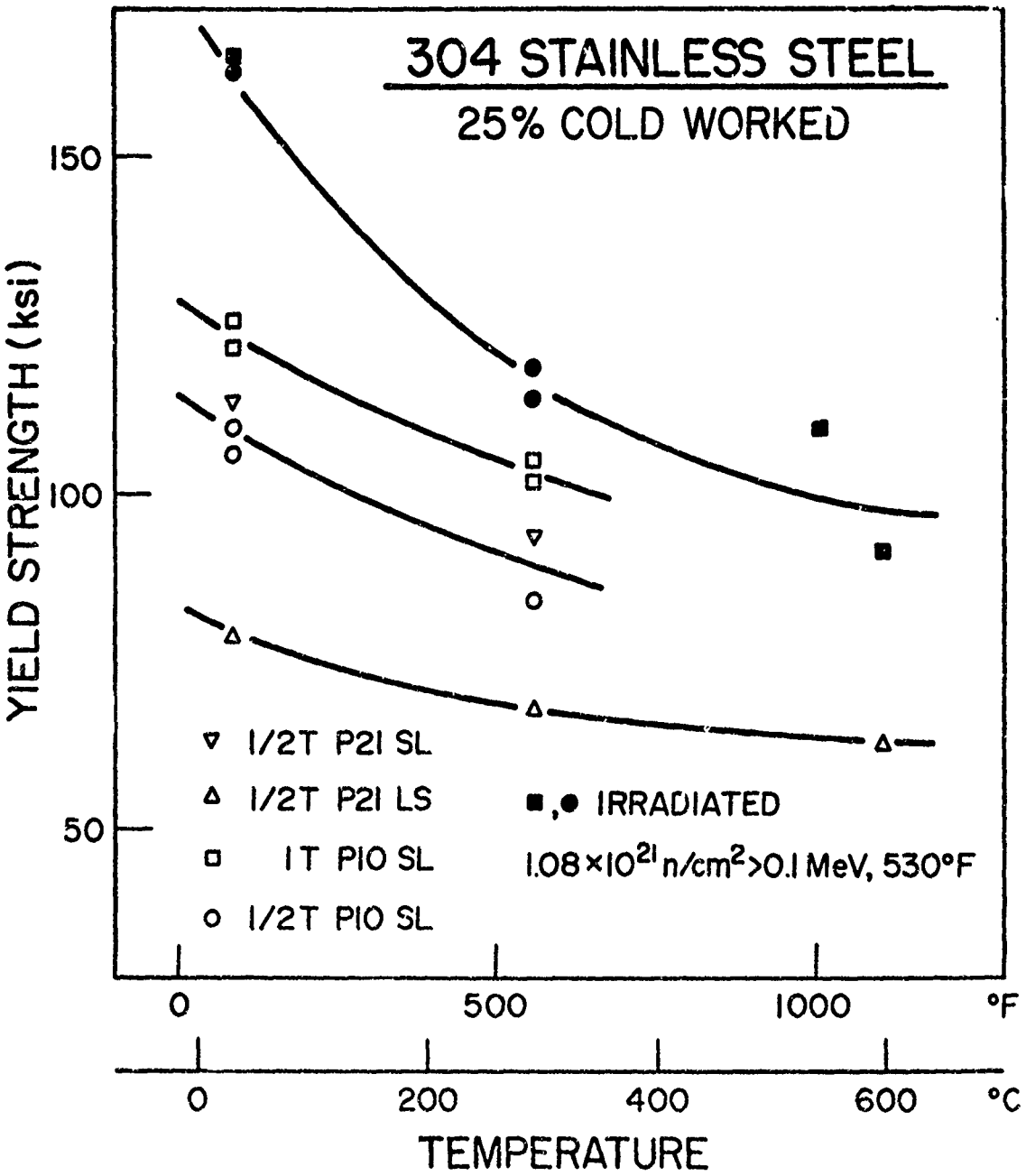

Fig. 3 - Ultimate tensile strength as a function of temperature for 25% cold worked stainless steel.

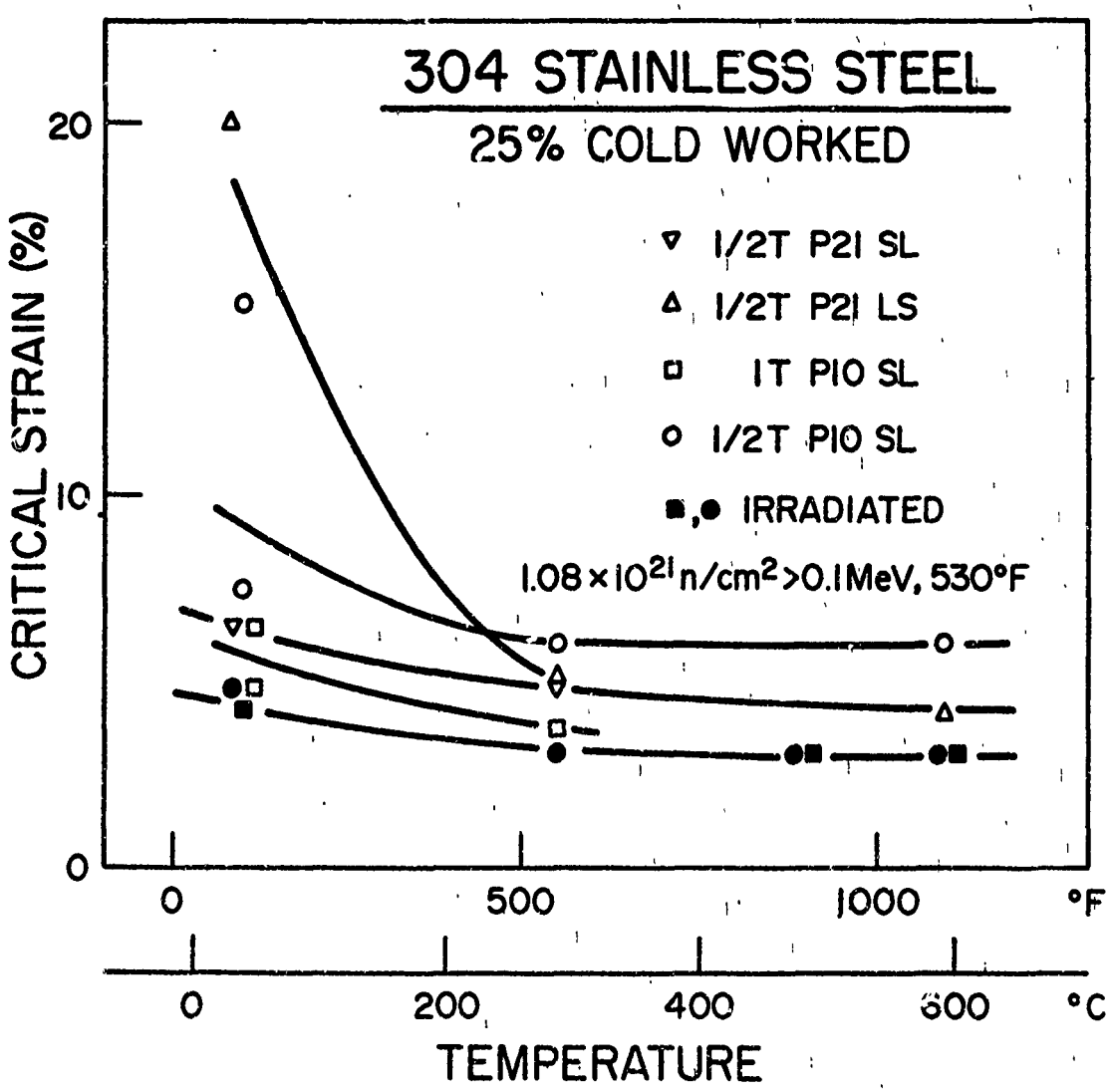

Fig. 4 - Critical strain as a function of temperature for 25% cold worked stainless steel.

$$e_c = \frac{1.176}{L/\Delta L - 0.8} \quad (1)$$

where L is the initial specimen length and ΔL is change in specimen length. This strain is then relatable to true longitudinal strain through considerations of constancy of volume. In this context, engineering longitudinal strain is approximately equal to twice the engineering diametral strain, and true longitudinal strain is essentially identical to twice the true diametral strain. The resulting true strain (ϵ) is found to be

$$\epsilon = 2\ell n\ (e/2 + 1). \quad (2)$$

Following this, the engineering tensile strain (e_t) and the true stress (σ) can be determined

$$e_t = (\exp\ \epsilon) - 1 \quad (3)$$

$$\sigma = (P/A)\ \exp(\epsilon^{-1}) \quad (4)$$

where P is the applied compressive load, and A is the initial specimen cross-sectional area. The critical strain and corresponding true stress found in the Considère construction define the UTS.

$$UTS = \sigma/(1 + e_t). \quad (5)$$

The trends observed in the compression testing are summarized below (Figs. 1-4). The variables considered are:

- temperature
- cold work vs anneal
- irradiation
- cold work procedure
- through thickness location
- specimen orientation

Temperature - The expected trend of loss of strength and work hardening coefficient with increase in temperature are consistently seen under all conditions examined.

Cold Work vs Anneal - Comparing the yield strength (YS) and UTS values (Figs. 2 and 3), it can be seen that the ratio of YS to UTS for the CW material is unity for the irradiated condition and very nearly unity for the unirradiated condition. However, the unirradiated, annealed material exhibits a ratio of approximately 0.4. The work hardening coefficients bear out these trends, i.e., n is small for CW material in general (typically .03 to .06) vs values of n from 0.3 to 0.6 for

annealed, unirradiated material (i.e., an order of magnitude larger than for the CW material).

Irradiation - An elevation in YS and UTS is shown in Figs. 2 and 3 for irradiated CW material. This elevation is more pronounced for the YS values than for the UTS. The effects of irradiation decrease with increasing temperature, especially in the case of the UTS values. The work hardening coefficient is decreased by irradiation to about one-half of its value in the initial condition.

Effect of Cold Work Procedure - In this study two pieces of material from the same plate were rolled to the same total reduction but within two different histories of percentage reduction per pass through the rolling mill. This may possibly have had an effect on the flow properties and thus might account for the slight variations noted between the YS and UTS values for the curves in Figs. 2 and 3 labeled 1/2TP10SL and 1/2TP21SL. The strain rate of the rolling process was not investigated in this study but may also have had some effect.

Through Thickness Location - The effects of the through thickness location of test specimens for CW material are seen in Figs. 2 and 3 as higher YS and UTS for the curves labeled 1TP10SL as compared to the curves labeled 1/2TP10SL. As a result of the cold forming characteristics of 304 SS and the capacity of the rolling mill used, material at the surface of the plate was more heavily cold worked compared to material at the plate 1/2T location.

Effect of Specimen Orientation - Some degree of preferred orientation for the annealed material is indicated by the YS dependence on directionality. This is seen in Fig. 1 as the values for YS curves 1/2TP21LS and 1/2TP10SL. The effect is not apparent in the UTS. A reversal of this directionality occurs in the instances of the CW SS, shown in Figs. 2 and 3 labeled as curves 1/2TP21LS and 1/2TP21SL; i.e., the compressive properties transverse to the primary rolling direction are higher than those parallel to the rolling direction. The effects of preferred orientation on the UTS become less perceptible at higher temperatures (near 1000°F, 538°C). This property dependence on orientation may be due to a combination of the Bauschinger effect and a crystallographic texturing as a result of directional rolling such that the slip systems in compression favor deformation in the primary rolling direction. To a lesser extent, this effect of material property dependence on orientation may also be attributable to mechanical texturing that results from elevated

temperature testing; this may produce carbide precipitation along the preferentially oriented grain boundaries. Such mechanical texturing is thought to be responsible for the smaller slopes of the curves representing surface material compared to the midthickness plate material.

Future development of flow properties for J-integral evaluation will include tensile as well as compression specimens. This will enable the Bauschinger effect to be determined for the subject steel.

J-Integral Evaluation Procedures

The J-integral specimens and test procedures are described in Reference 1. Briefly, the specimens examined thus far are 3-point bend beams having the same planar dimensions as a Charpy bar but only half its thickness (Fig. 5). The experiments considered here have a ratio of crack length to specimen width (a/W) of approximately 0.3. Figure 5 illustrates load-deflection traces for irradiated 304 SS in the annealed and 25% CW conditions. The predicted curves are based on the Bucci approximations described in Reference 1. The rising dashed lines represent the calculated load-deflection behavior based upon an elastic beam, of the same dimensions as the test piece, and incorporating a plane stress plastic zone size correction. The horizontal dashed curve is the plastic limit load P_L calculated from the relationship:

$$P_L = 1.456\ \sigma_{ts}\ \frac{B}{S}\ (W-a)^2 \qquad (6)$$

where σ_{ts} is the tensile strength, S is the span between specimen supports, and the other terms relate to the specimen geometry as illustrated in Fig. 5.

The calculations of the dashed curves, described in the prior progress report[1], were based on approximations of the yield and tensile properties. Comparison of these estimates with the actual flow properties described above resulted in a noticeable modification of the predicted curves only for the CW material. For this material in the irradiated condition it was surprising that the yield and tensile values were identical. Normally such behavior is indicative of low ductility. This is confirmed by the instability strains which, for the irradiated CW material, are an order of magnitude below that of the unirradiated, annealed material. In general, it was found that the measured curves followed the predicted curves better if a plane stress plastic zone correction was used as opposed to a plane strain correction. Inability of the specimens to reach the predicted limit load is attributed to the fact that the crack extended, either by slow stable

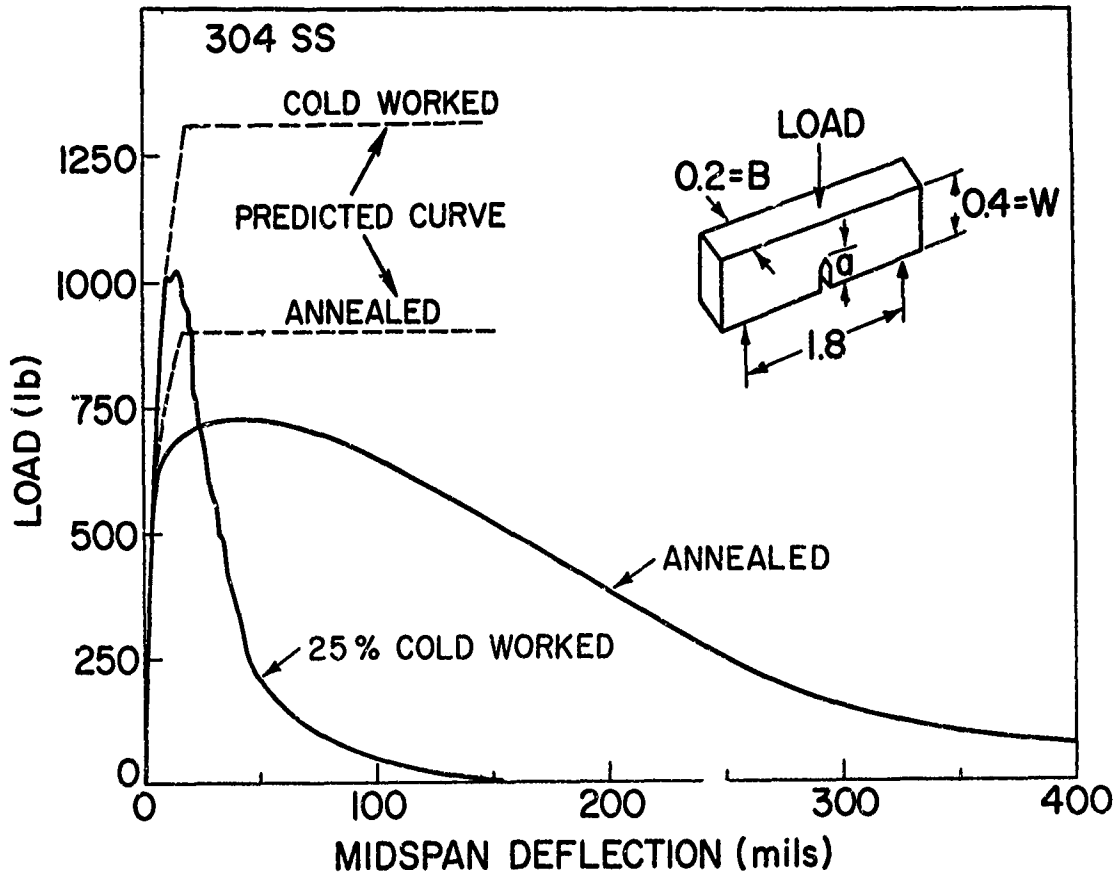

Fig. 5 - Comparison of load-deflection records for stainless steel specimens irradiated ataapproximately 535°F (279°C) to a fluence of 1.08×10^{21} n/cm^2 > 0.1 MeV and tested at 550°F (288°C). The predicted curves (dashed) are based on an analytical model that does not consider the slow crack extension which may take place (under rising load) before maximum load is attained. The failure of the experimental curves (solid) to reach the predicted maximum loads is therefore an indication of this phenomenon.

growth or by a local instability phenomenon, and the load supporting ligament was thereby reduced.

The preceding progress report[1] discussed the method of Bucci et al which was used to estimate the value of J using only one specimen. Two other approximate methods are of interest and are described below. These materials are both based on unpublished notes by Rice and Paris and consider a deeply notched beam in pure bending.

Estimation Method No. 1 - This method is based on an expression for K for a beam in bending due to Wilson:

$$K = \frac{4M}{(W-a)^{3/2}} \tag{7}$$

where K is the stress intensity factor and M is the bending moment. Incorporating Eq. 7 with Castigliano's theorem, a plastic zone correction and a theorem of Rice's which relates J to the bending moment, it is possible to derive the following expression for J:

$$J = \frac{P\delta}{B(W-a)} \left[1 - \alpha D^2 \left(\frac{P}{P_L} \right)^2 \right] \tag{8}$$

where P and δ are the respective load and deflection at instability, P_L is the plastic limit load, and αD^2 is an experimentally derived constant whose value is less than 0.5 and most probably equal to 0.36 according to Paris. This method has the advantage that J can be calculated in a simpler fashion than with the Bucci method.

Estimation Method No. 2 - This procedure is based directly on a theorem of Rice which relates the bending moment and angle of rotation of the notched beam using dimensional analysis and the equation for J,

$$J = \int_0^M \left(\frac{\partial \theta_{tot}}{\partial a} \right)_M dM \tag{9}$$

where M is the bending moment, θ_{tot} is the total angle of rotation. From this Rice has shown that

$$J = \frac{2A}{B(W-a)} \tag{10}$$

where A is the area under a load deflection trace for a notched beam up to the point of crack instability.

In applying these estimation procedures, expression 10 gives the simpler physical interpretation of J. It is apparent that large J values will be obtained from specimens

having large areas under their load deflection traces up to maximum load. Also, it is apparent from Eq. 10 that J does not depend on the total energy absorption of a completely fractured specimen. This point is important and it calls for a careful interpretation of J when comparisons are made with other methods of toughness evaluations such as the Charpy-V and dynamic tear tests which are based on total energy absorption of the fractured specimen.

Use of Eq. 10 enables one to obtain a physical interpretation of the load deflection traces in Fig. 5. If it is assumed that the maximum load and the corresponding specimen deflection define the point of crack initiation, then it is apparent that the area up to maximum load for the annealed material is several times larger than for the CW material; the J value for the annealed material is therefore proportionately greater than that for the CW steel. Qualitative assessments of the elastic plastic toughness of various materials can thus be directly obtained from the areas associated with the load-deflection records.

J-Integral Trends

The values of the J integral computed by the various procedures described are summarized in Table 1. J is computed both at the conditions of maximum load and at the conditions corresponding to crack initiation, when the latter could reasonably approximated. It must be remembered that the crack can extend at a load less than the maximum load and thereby exhibit a slow stable tearing behavior. Unfortunately, simple methods for assessing the point of crack initiation are not readily available and this condition has been approximated as described in Reference 1. It must also be recalled that the value of J is quite sensitive to the value of specimen deflection used in the calculation. Therefore, a large difference in specimen deflection from the point of crack initiation to the point of maximum load will result in a large difference in J even if the loads at the two points are similar. The structural interpretation of this behavior presents a challenge to the successful application of J.

Several observations have been made from the data presented in Table 1.

1. All of the methods used to calculate J give approximately the same results. Some interpretation of the results using the methods of Eqs. 8 and 10 is possible. The technique used here was to base all calculations on the original crack lengths before the specimen was loaded. This procedure may not result in the same value of J for

TABLE 1

Summary of J-integral Values for Stainless Steel Plate and Weld Metal

Code	Spec. No.	Material[a]	Notch[b] Prep.	Test Temp. (°F)	J by Eq. 10 Crack Initiation (in.lb/in.^{2})	J by Eq. 10 Max. Load	J by Eq. 8 Crack Initiation	J by Eq. 8 Max. Load	J by Bucci Method Crack[c] Initiation	J by Bucci Method Max.[c] Load
P-10-34	1	I,A, SL	F	550	105	894	100	618	75-82	880-960
P-10-49	2	I,A, SL	F	550	-	548	-	426	-	530-600
P-10-33	3	I,CW,SL	F	550	247	366	265	341	190-215	310-340
P-10-36	4	I,CW,SL	F	550	177	222	216	250	160	215
P-10-45	5	U,CW,SL	F	550	-	325	-	330		
P-10-19	6	U,A, SL	F	550	-	2412	-	1760		
P25-52	7	U,A, SL	P	RT	1682	7172				
P25-14	8	U,A, LS	P	RT	2085	9446				
P25-15	9	U,A, LS	M	RT	2287	8055				
P25-55	10	U,A, SL	P	1000	-	1765				
P25-7	11	U,A, LS	P	1000	-	2618				
P25-8	12	U,A, LS	M	1000	-	3347				
P26-7	13	U, Weld	P	RT	660	974 est.				
P26-5	14	U, Weld	P	1000	-	1045				

[a] 304 stainless steel or 308 stainless steel weld
I - irradiated to fluence of 1.08×10^{21} n/cm^2 >0.1 MeV
U - unirradiated
A - annealed
CW- cold worked
LS and SL refer to specimen orientation

[b] F - fatigued
M - machined with 60° tip angle
P - machined with knife-pressed tip

[c] Range of values for plane stress or plane strain calculations.

the case where some slow, stable crack growth has taken place, say up to maximum load. The limits of allowable growth consistent with meaningful J calculations have yet to be determined.

2. Considering the J values at maximum load, the toughness of the irradiated CW material is significantly less (i.e., 1/3 to 1/4) than that of the irradiated annealed plate (Specs. 1-4). Comparisons of the CW and annealed material on the basis of crack initiation may be somewhat misleading. For example, J at initiation for the irradiated, annealed material (Spec. 1) is around 100 in.lb/in.^{2} whereas that for the CW material (Spec. 3) is more than twice this value at initiation, thereby implying the CW material is the tougher. However, from a qualitative structural viewpoint, it is apparent that the annealed material is tougher than the CW material. The argument is that the annealed material can exhibit some slow tearing and still support additional load (see Fig. 5), whereas the CW material cannot. Clearly, the slow growth phenomenon holds the key to resolving this question.

3. Comparisons of the irradiated and unirradiated annealed specimens tested at 550°F (288°F) (Specs. 1, 2, and 6) indicate a significant drop in J due to irradiation. A similar comparison for the CW material (Specs. 3, 4, and 5) shows that while J of this material is less than that of the annealed specimens, relatively little additional degradation, above that imparted by the CW, is due to irradiation.

4. Comparison of unirradiated, annealed plate tested at room temperature (RT) (Specs. 7-9) and 1000°F (538°C) (Specs. 10-12) shows a large drop in J at the higher temperature, based on the maximum load calculation. In addition, it is to be noted that the J values for initiation for the RT tests (Specs. 7-9) are much lower than the values at maximum load, similar to the behavior of the irradiated, annealed specimens (Specs. 1,2). Note that the notches in Specs. 7-14 were not fatigue cracked and so comparison of results for these specimens with those containing fatigue cracks may be somewhat different from a comparison based upon one type of notch preparation.

5. Comparison of the unirradiated 308 SS weld metal specimens (Specs. 13 and 14) with the annealed 304 SS plate specimens tested at RT and 1000°F (538°C) (Specs. 7-12) shows the J values for the weld to be significantly lower than those for the plate. In addition, the results of weld metal tested at RT and 1000°F (Specs. 13 and 14) suggest little effect of temperature whereas this is not the case

for the plate as discussed above. However, the J for the RT weld (Spec. 13) has been estimated from a poor load-deflection trace and additional data are required to draw a conclusion concerning the effect of temperature on the toughness of the weld metal.

B. Fatigue Crack Propagation in Neutron Irradiated Stainless Steel Weldments

P. Shahinian, H. E. Watson, and H. H. Smith

An assessment of structural performance of nuclear reactors should consider the properties of the welds as well as the component materials. Of particular interest is the resistance of the weld metal to crack propagation under cyclic loading because of the tendency for small cracks to form in the welds. In service these cracks can grow to a large enough size to cause sudden failure

In an initial phase of an investigation on unirradiated Types 304 and 316 stainless weldments we found that, in general, resistance to crack propagation of weld metal is at least as high as that of the base metal. Postirradiation fatigue resistance of identical weldments has now been determined.

The Types 304 (Type 308 weld metal) and 316 SS S/A weldments (Table 2) were irradiated in the EBR-II at ~760°F (404°C) to a fluence of $\sim 1.2 \times 10^{22}$ n/cm^2 >0.1 MeV. Fatigue tests were then conducted at 800 and 1100°F (427 and 593°C). The single-edge-notch fatigue specimens with a 0.5-in. thick, 2.5-in. wide test section containing side grooves were cycled at 10 cpm in cantilever bending under zero-to-tension loading to a constant maximum load. For the in-cell tests, crack length was measured by means of a remote high-resolution television system. The rates of crack growth were determined by measuring the slopes of the plotted curve of crack length vs number of cycles.

For analysis of the fatigue crack growth behavior the rates of crack growth were plotted as a function of stress intensity factor range on logrithmic coordinates. Irradiation of the weld metal resulted in higher crack growth rates for both Types 308 and 316 steel, as demonstrated in Fig. 6. The rate increase was generally no more than a factor of 2 except at growth rates of $<1 \times 10^{-5}$ in./cycle where it was greater. For the Type 316 weld metal, in fact, the range of variation in growth rates among irradiated, unirradiated, 800°F, and 1100°F data was usually within a factor of 2 at rates above 1×10^{-5} in./cycle. Further, the crack growth rates for irradiated Types 308 and 316 weld metal at 1100°F (593°C) were essentially equivalent for a given stress intensity factor range.

Table 2

Chemical Compositions of AISI Type 304 and Type 316 Submerged Arc Weldments

Material	Chemical Composition (wt-%)								
	C	Mn	P	S	Si	Cr	Ni	Mo	B
Type 304 Weldment									
Plate	0.056	1.6	0.028	0.014	0.54	18.5	9.3	0.7	<0.0006
Weld (Type 308)	0.030	1.60	0.021	0.010	0.68	21.0	9.7	0.2	<0.0006
Type 316 Weldment									
Plate	0.059	1.8	0.014	0.009	0.45	17.4	13.4	2.7	0.0006
Weld (Type 316)	0.055	2.1	0.023	0.009	0.65	18.8	11.7	2.7	<0.0006

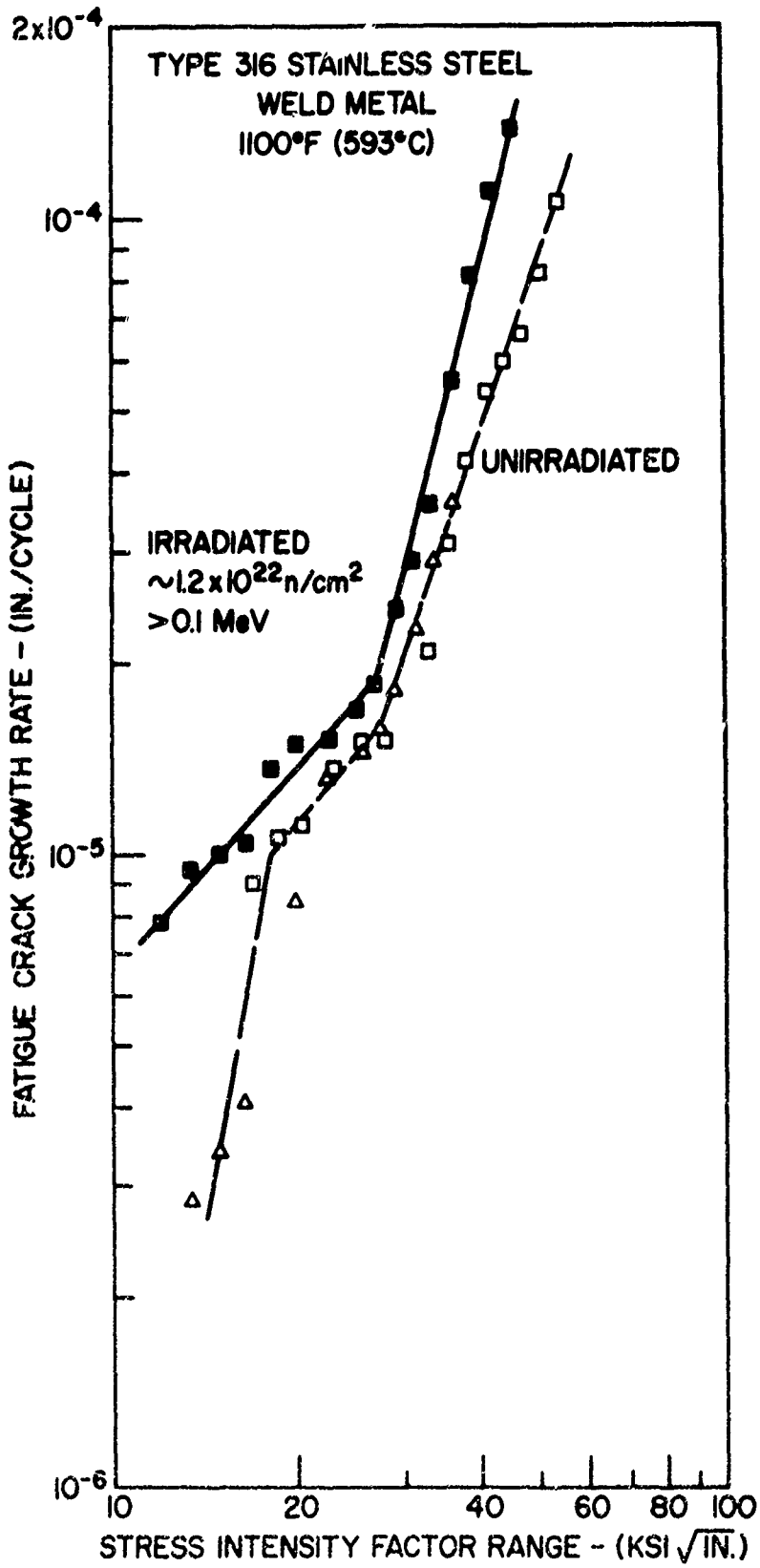

Fig. 6 - Effect of neutron irradiation on fatigue crack growth rates in Type 316 weld metal at 110°F (593°C)

A comparison between crack growth rates in irradiated weld and base metals was made. As shown in Fig. 7, there is very little difference between rates in Type 308 weld metal and Type 304 base metal at 1100°F (593°C). However, for the Type 316 weldment the results were inconsistent. At 800°F the growth rates appear to be slightly higher for the weld metal while at 1100°F the rates are higher for the base metal.

In general it has been found that neutron irradiation in the EBR-II reduces slightly the resistance to crack propagation of Types 308 and 316 weld metals at elevated temperatures.

C. Exploratory Assessments of A508 Forging Radiation Resistance

J. R. Hawthorne

An appreciable amount of information has been developed on the irradiation response characteristics of A533-B plate and weld metals as used in current water reactor vessel construction. Available data indicate that significant variability in elevated temperature (550°F, 288°C) radiation embrittlement resistance is common for these materials and that residual elements content is a key factor in their properties retention in nuclear environments. Comparable information on the performance of irradiated A508 forgings has not been developed although increasing use of such forgings in reactor vessel fabrication is projected. Accordingly, exploratory studies on the irradiation behavior of A508-2 and A508-4 forgings were undertaken.

Preliminary assessments of two A508-2 forgings (12-in. and 9-1/2-in. thick) and one A508-4 forging (23-1/2-in. thick) have been completed. The forgings were produced commercially. Available information on individual chemical compositions is summarized in Table 3. Preirradiation properties are summarized in Table 4. Specimens in each case were removed from the forging quarter thickness location. Charpy-V (C_V) specimens from Forging Code 1 were irradiated to 3.0×10^{19} n/cm^2 >1 MeV at 550°F (288°C); C_V specimens from Forging Codes 2 and 3 were irradiated simultaneously to 2.2×10^{19} n/cm^2 at 550°F (288°C). Figures 8-10 summarize pre- and postirradiation results.

Before irradiation, both A508-2 forgings showed comparable drop weight nil ductility transition (NDT) temperatures (Table 4). However, significant differences are noted in the average C_V energy level at the NDT temperature (44 vs 100 ft-lb) and the C_V 30 ft-lb transition temperature of these forgings (20 vs -40°F, -7 vs -40°C). Therefore, the results demonstrate well that an arbitrary C_V "energy fix" cannot be

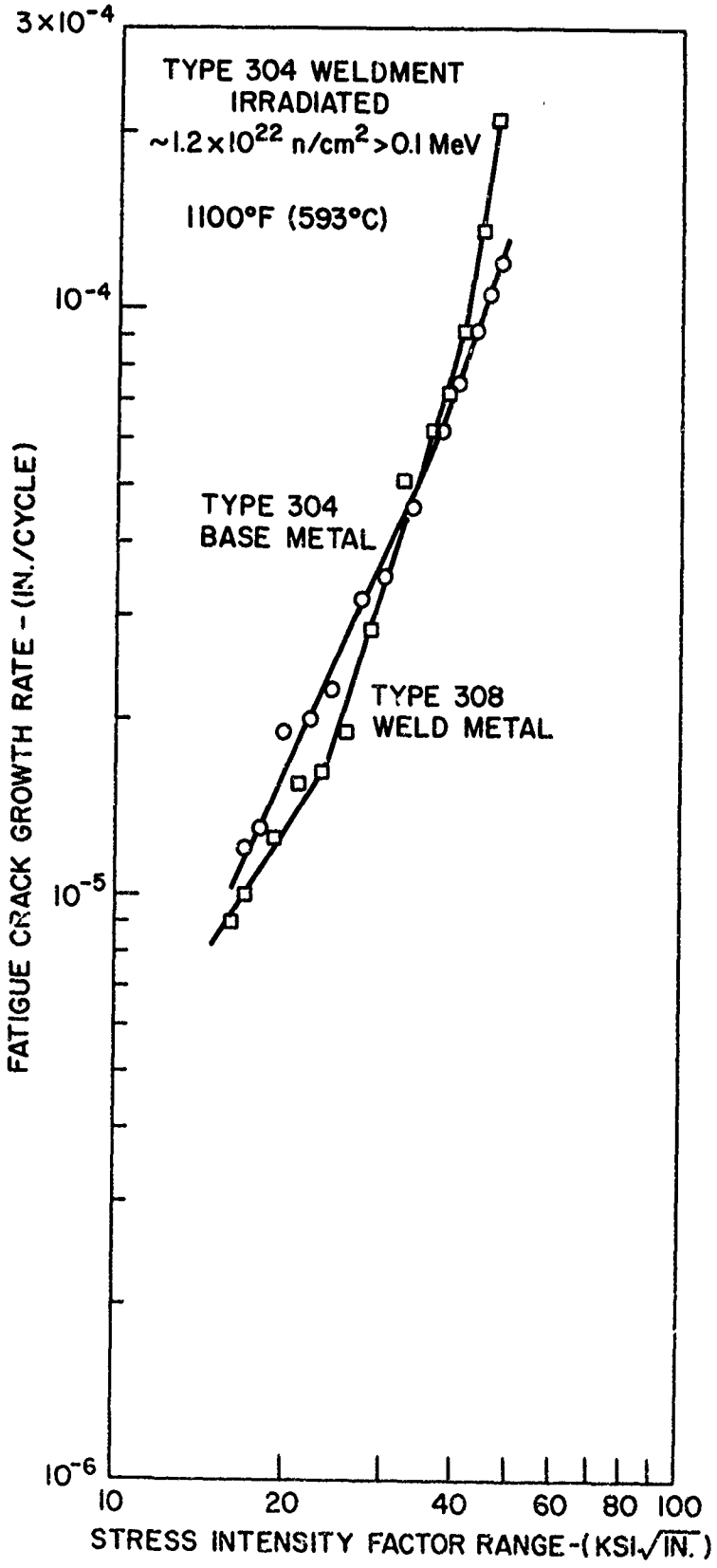

Fig. 7 - Fatigue crack growth rates in Type 304 stainless steel weldment at 1100°F (593°C)

Table 3

Chemical Composition of Forgings

Forging	Code	Composition (wt-%)*									
		C	Mn	Si	P	S	Ni	Cr	Mo	Cu[a]	V
A508-2 (12-in.)	1	.19	.70	.34	.011	.011 (.009[a])	.89	.39	.56	.13	<.01
A508-2[b] (9-1/2-in.)	2					.008[a]				.09	
A508-4	3	.15	.34	.21	.007	.011	3.46	1.72	.48	c	.01

*-Courtesy supplier except as noted
a-NRL determination
b-Additional analyses underway
c-Not yet determined

Table 4

Notch Ductility and Tensile Properties of Forgings (Preirradiation Condition)

Forging	Code	NDT (°F)	NDT (°C)	Charpy-V 30 ft-lb Temp. (°F)	Charpy-V 30 ft-lb Temp. (°C)	Charpy-V Energy at NDT (ft-lb)	Charpy-V Upper Shelf (ft-lb)	Yield Strength[a] (0.2% offset) (ksi)	Tensile Strength (ksi)
A508-2 (12-in.)	1	50	10	20	-7	44	137	80.5	100.5
A508-2 (9-1/2-in.)	2	40	4	-40	-40	100	161	69.8	91.9
A508-4 (23-1/2-in.)	3	-	-	-110	-79	-	157	84.5	102.0

[a]-0.252-in. gage diameter specimens except as noted
[b]-0.505-in. gage diameter specimen

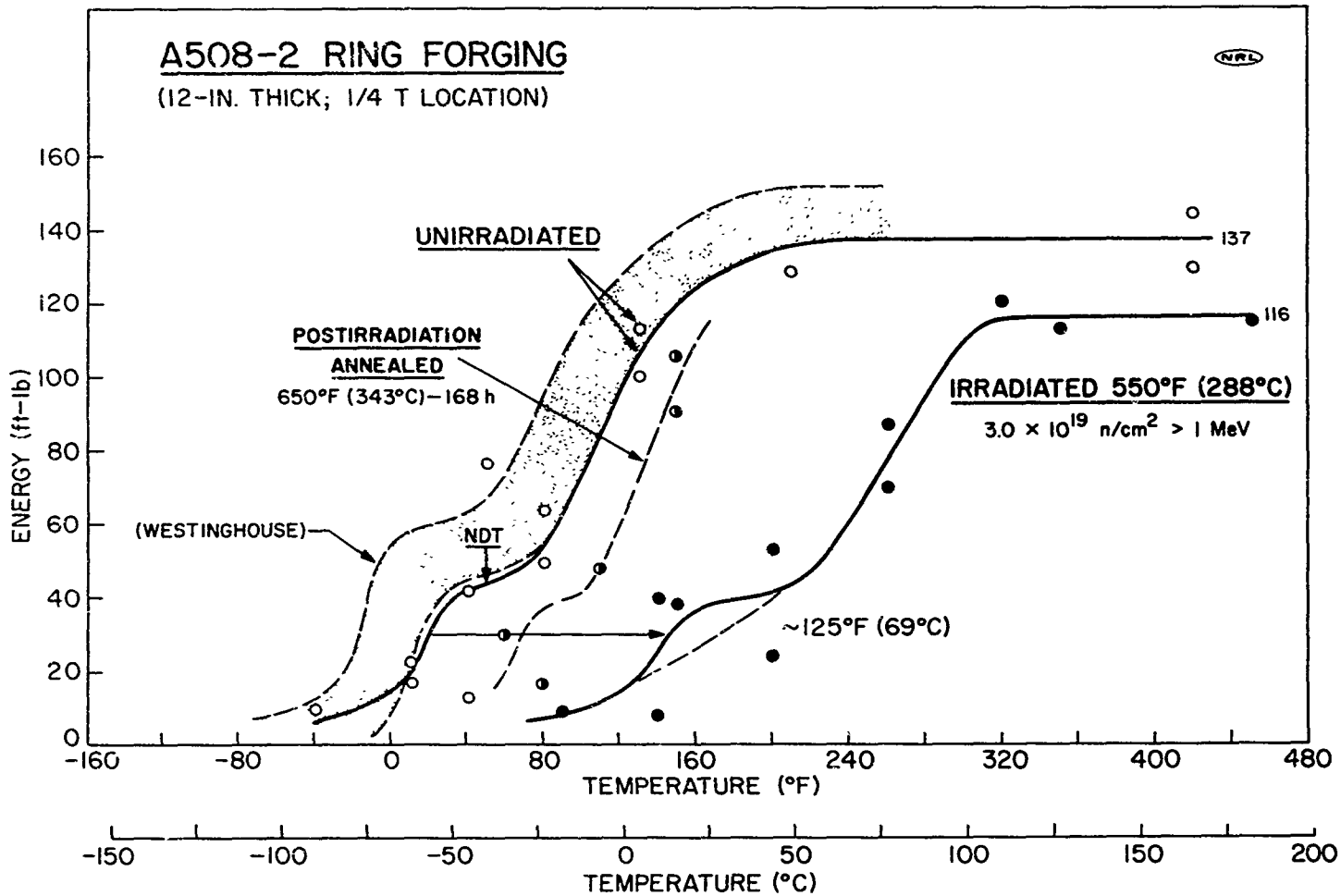

Fig. 8 - Charpy-V notch ductility of the 12-in. thick A508 Class 2 ring forging (Code 1) before and after irradiation. The shaded band refers to Charpy-V data developed separately by Westinghouse for the unirradiated condition. An NDT determination by the drop weight test method is also indicated. Limited data for the 650°F (343°C) postirradiation annealed condition are given by the half-filled symbols.

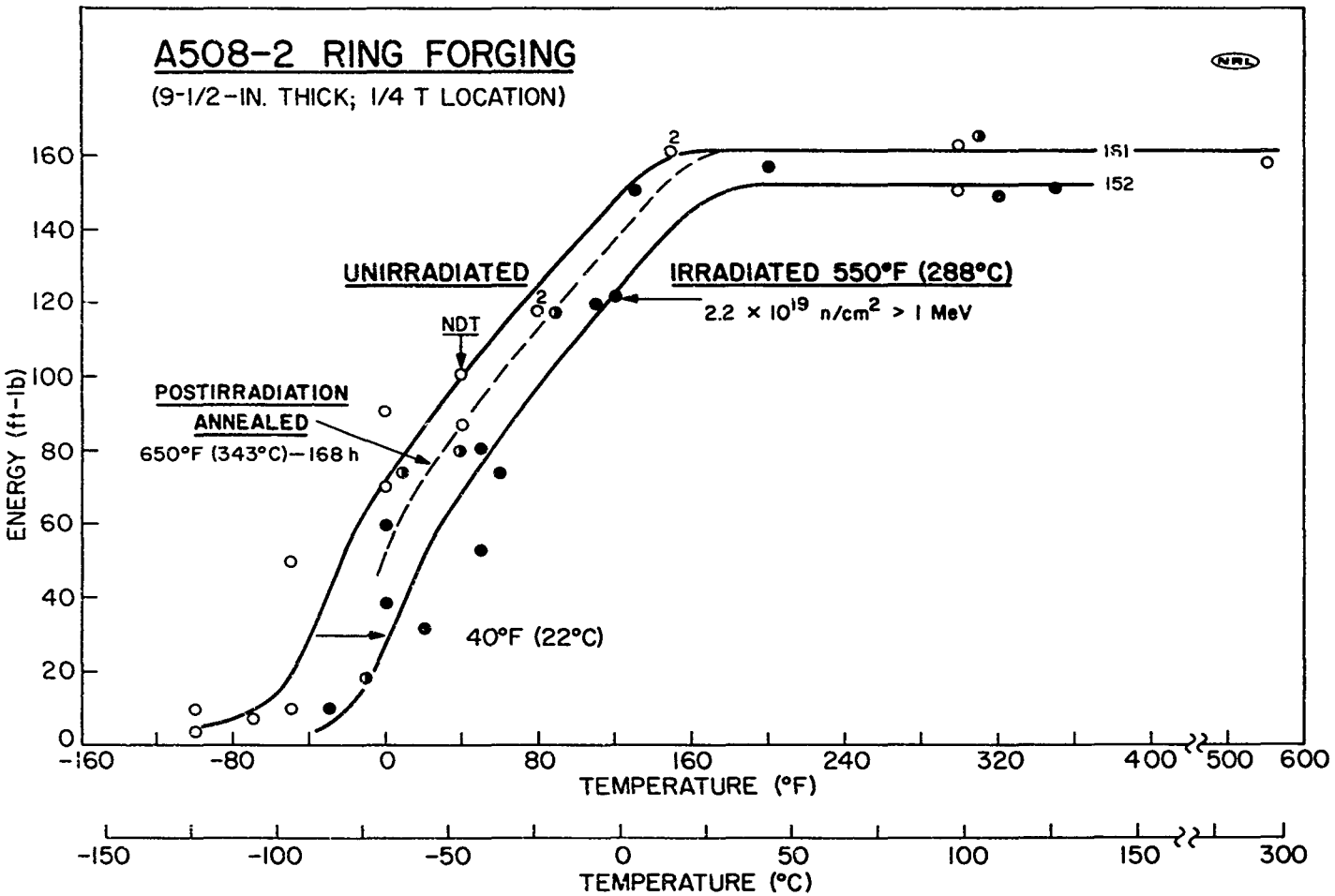

Fig. 9 – Charpy-V notch ductility of the 9-1/2-in. thick A508 Class 2 ring forging (Code 2) before and after irradiation. An NDT determination by the drop weight test method is also indicated. The half-filled symbols refer to the 650°F (343°C) postirradiation annealed condition.

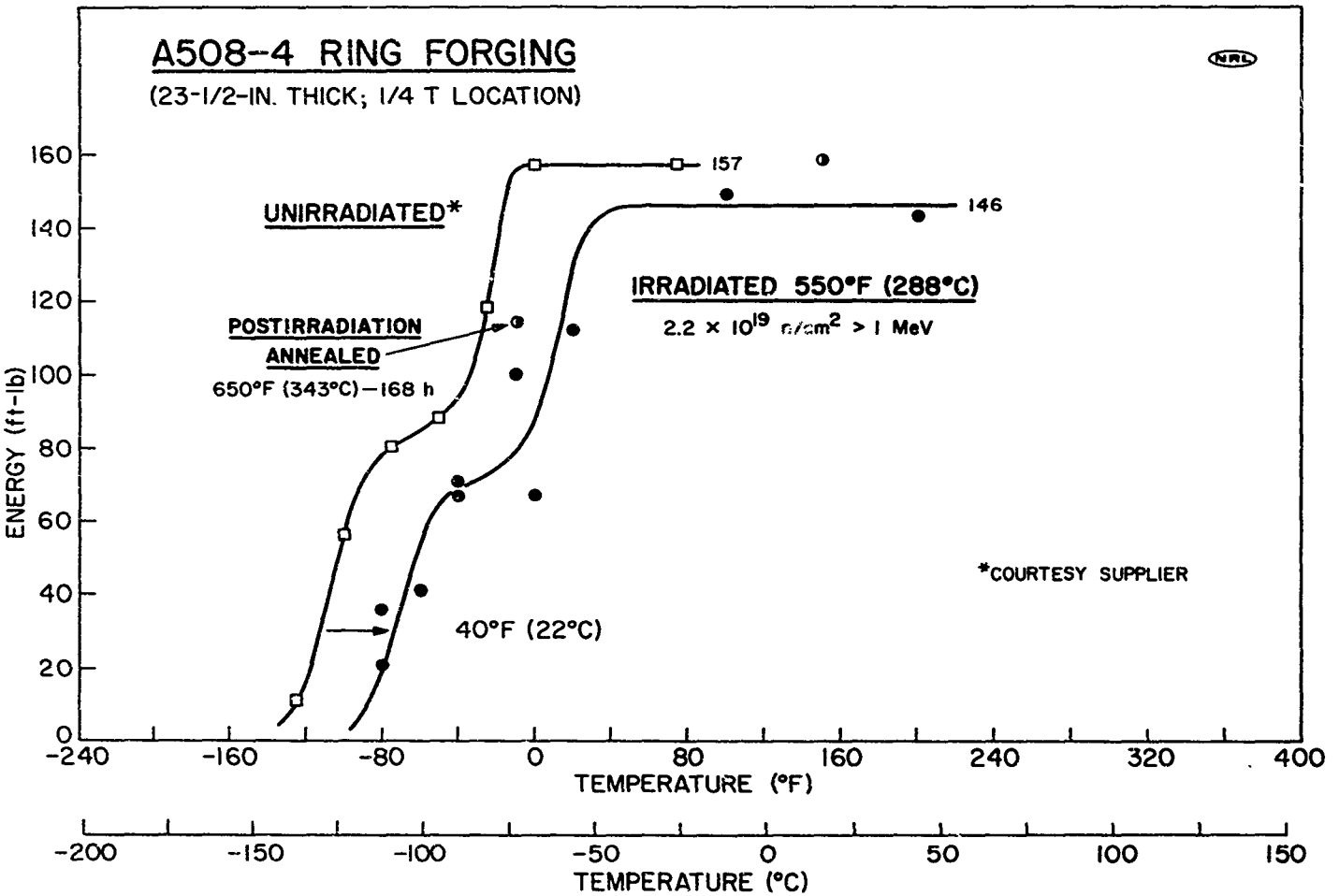

Fig. 10 - Charpy-V notch ductility of the 23-1/2-in. thick A508 Class 4 ring forging (Code 3) before and after irradiation. The half-filled symbols refer to the 650°F (343°C) postirradiation annealed condition.

used to predict the NDT temperatures of A508-2 forgings. (Stock was not available for an NDT determination for the A508-4 forging .) All three forgings exhibited relatively high C_V upper shelf levels and comparable yield strength levels. Thus, property differences which would tend to explain the high "energy fix" for NDT in one case are not evident. It is noted, however, that Forging Code 2 did feature a combination of the lowest yield strength and highest upper shelf for the series.

With irradiation, a relatively large increase in C_V 30 ft-lb transition temperature (125°F, 69°C) was found for Forging Code 1 (Fig. 8). The irradiation of Forging Codes 2 and 3, on the other hand, produced only a small shift in the C_V 30 ft-lb transition (40°F, 22°C). On evaluating individual results with the performance trend for A533-B[5], the radiation embrittlement resistance of Forging Code 1 appears equal to the average resistance exhibited by different plates and welds of A533-B at the 3.0×10^{19} n/cm^2 fluence. The performance of Forging Codes 2 and 3, however, is equal to the best performance noted for A533-B plates and welds (unimproved commercial production). Accordingly, A508 forgings appear to have similar radiation response characteristics to those of A533-B steel plate.

Chemical composition determinations to help establish the cause(s) of the poorer radiation embrittlement resistance of Forging Code 1 relative to Forging Codes 2 and 3 are only partially complete. The copper and phosphorus contents of Forging Code 1 were not abnormally high. However, the copper content (.13%) was higher than the copper content of Forging Code 2 (.09%) and the phosphorus content (.011%) was higher than the phosphorus content of Forging Code 3 (.007%). From this partial analysis, residual impurities content would appear to be equally important to the radiation performance of forgings as to plate and weld metals. Separately, it was noted that the radiation resistance of Forging Code 1 was comparable to that of a well documented A533-B plate with .13% copper and .008% phosphorus[5].

Limited assessments of 650°F (343°C)-168 hr postirradiation annealing response were made with surprising results. A recovery in 30 ft-lb transition temperature of less than 40% was anticipated in light of the 650°F (343°C) annealing response shown by the ASTM A302-B reference plate[6]. Forging Code 1, however, showed a transition temperature recovery on the order of 70%. Forging Codes 2 and 3, although having only minor radiation embrittlement, also indicated an unexpectedly high tendency to respond to this treatment. Since intermediate in-service annealing at 650°F (343°C) is considered within the capacity of many current reactor vessel

designs, further investigation of forging response to 650°F (343°C) postirradiation heat treatment may be of interest.

Studies of irradiation performance characteristics of A508 forgings are continuing. Efforts for the next quarter will include dynamic tear assessments of the preirradiation condition for Forging Codes 1 and 2.

II. RADIATION DAMAGE MECHANISMS

A. A Parametric Study of the Vacancy Trapping During Irradiation

F. A. Smidt, Jr. and J. A. Sprague

Background

Past work has shown that the presence of small amounts of impurities, especially copper, have a marked effect on irradiation hardening and embrittlement of pressure vessel steels[7], and these changes can be related to the defects formed during irradiation[8]. The range of irradiation temperatures at which the phenomenon occurred indicated a vacancy interaction with the copper atoms was most likely responsible for the behavior. To study this phenomenon in more detail, a less complex material than the pressure vessel steel was desirable so a series of iron alloys made up of pure zone refined iron and 0.3 at.% of copper, vanadium, nickel, and phosphorus and 0.1 at.% carbon were prepared and irradiated under a number of conditions. The first observations of a modification in the defect microstructure as a result of solute additions were at a fluence of 8×10^{20} >0.1 MeV and an irradiation temperature of 280°C (535°F)[8]. These results showed enhanced nucleation of dislocation loops in the copper bearing material and suppression of void formation in the vanadium and phosphorus alloys. More recently, the same series of alloys was irradiated in the EBR-II at a temperature of 525°F (975°F) to a fluence of 8.5×10^{21} n/cm^2 >0.1 MeV. It was found that void nucleation in the Fe-.3V alloy had been completely suppressed while void numbers and sizes in the phosphorus alloy were lower than in the nickel and carbon alloys and the pure iron. Since the composition of these materials differs only in the specific solute element added and they were irradiated under identical conditions, it is apparent that the effects observed are due to the presence of a specific solute element. To resolve the question of the mechanism of radiation damage in these materials, it is necessary to understand the effect of the vacancy-impurity interaction on the steady state defect concentration and how this in turn will influence the nucleation of vacancy aggregates in these materials. This quarterly report gives the result of a modeling study to predict the effect of vacancy trapping by impurity atoms on the steady defect concentration and shows some calculations of the effect of this reduction in vacancy concentration on homogeneous nucleation rates for voids and vacancy loops.

Kinetic Equations

The kinetic equations for defect concentration originally used by Damask and Dienes[9] and, more recently, by Weidersich[10], and Harkness and Li[11] were the starting point for our calculations of vacancy concetration. Additional terms were added to account for the presence of vacancy-impurity atom complexes. The basic equations are shown below as Equations 11 and 12.

$$\frac{dN_v}{dt} = 0 = G_v^* - \bar{Q}_v\left(\nu_v^F N_v^F + \nu_v^T N_v^T\right) - Z\frac{\nu_i}{N} N_i\left(N_v^F + N_v^T\right) \quad (11)$$

$$\frac{dN_i}{dt} = 0 = G_i - \bar{Q}_i \nu_i N_i - Z\frac{\nu_i}{N} N_i\left(N_v^F + N_v^T\right) \quad (12)$$

$$\frac{dN_v^T}{dt} = 0 = \left(ZX_T - \frac{N_v^T}{N}\right) \nu_n^F N_v^F - \nu_v^T N_v^T - Z\frac{\nu_i}{N} N_i N_v^T \quad (13)$$

$$G_v^* = G_v + \bar{Q}_v \nu_v^F N_v^{eq}$$

G_j = defect production rate (dpa/sec)

$\bar{Q}_j = \frac{Q_j}{\nu_j}$ = sink loss probability

$$\bar{Q}_v^{disl} = \frac{2\pi\rho}{\mathrm{Log}(r/r_c)}$$

$$\bar{Q}_i^{disl} = \frac{2\pi\rho}{\mathrm{Log}\,(r/r_c + \Delta r_c)}$$

$$\bar{Q}_{v,i}^{gb} = \frac{3v_j N_j a^2}{r_{gb}\, r}$$

ρ = disl. density
r = sink separation
r_c = core radius
$\Delta r_c = .07ba^3\ \mu\epsilon/kT$
ϵ = 0.1, misfit parameter

ν_j = jump frequency

$\nu_j^T = \nu_j \exp(-E_B/kT)$ = jump frequency for trapped defect

N_j = number of defects

N = atoms/cm^3

X_T = impurity concentration

These equations are basically the same as used in previous investigations but have additional terms for recombination of interstitials with trapped vacancies. The third equation is the balance equation for formation and loss of trapped vacancies. The first term in Eq. 13 involves the formation rate of trapped defects, which is the product of the atom fraction of empty trap sites times the frequency with which they are encountered by migrating vacancies. The second term takes account of loss of trapped defects by thermal detrapping, and the third term accounts for the loss of trapped vacancies by recombination.

Equation 13 can be solved for α, the fraction of occupied trap sites, as shown in Eq. 14:

$$\alpha = \frac{X_v^T}{ZX_T} = \left[\frac{1}{1 + \frac{Z\nu_i N_i}{\nu_v N_v} + \frac{1}{X_v \exp(E_B/kT)}} \right] \quad (14)$$

it should be noted that in the case of small binding energies the last term of the denominator will completely dominate the expression, and α will be given by $X_v \exp(E_B/kt)$. A special case of this situation is for $E_B = 0$, in which case the fraction of sites occupied is simply the atom fraction of vacancies, X_v. For strong binding energies the last term in the denominator becomes small and can be ignored. The second term in the denominator approaches Z since $\nu_i N_i \approx \nu_v N_v$ and the ratio approaches one and, therefore, α approaches $1/(1 + Z)$. For most cases of interest, i.e., binding energies less than .5 ev and temperatures above 0.3 T_m, the absolute melting point, the weak binding approximation will give very good estimates of the vacancy concentration. With the weak binding approximation for the trapped vacancy concentration, one can substitute into Eqs. 11 and 12, solve for the interstitial concentration in terms of the free vacancy concentration, and finally, obtain a quadratic equation for the free vacancy concentration.

Calculations show that vacancy trapping decreases the free vacancy concentration, decreases the interstitial concentration, but of course increases the total vacancy (trapped plus free) concentration. In cases of strong binding, it is conceivable that larger aggregates could build up from the vacancy-impurity complex. We have considered the formation of di-vacancies trapped at an impurity atom, however, and find that for binding energies less than 0.5 ev and an additional 0.2 ev attraction between vacancies, the concentration of impurities with two vacancies is negligible. We therefore conclude that only free vacancies will enter into nucleation processes and the trapped vacancies are ignored in the analysis which follow.

Figure 11 shows the vacancy concentration in atom fraction as a function of temperature for irradiation under steady state conditions in a thermal reactor where a typical production rate is assumed to be 9×10^{-9} displacements per atom (dpa) per second. The upper curve shows the vacancy concentration without traps while the lower curve considers the effect of 0.6 at-% of trap sites, i.e., .075 at-% impurities surrounded by eight trap sites for each impurity. We have also assumed the binding energy, 0.5 ev, a dislocation density of 10^7 disl/cm^3, 0.33 ev migration energy for interstitials and 1.0 ev migration energy for vacancies. As can be seen in the figure, vacancy trapping decreases the steady state vacancy concentration anywhere from two orders of magnitude at temperatures around 500°K to a factor of about 3 or 4 near the intersection point with the thermal vacancy concentration at high temperatures.

Nucleation

The next question of interest, therefore, is how much of an effect this depression of the vacancy concentration can have on the nucleation rate for voids or vacancy loops. To address this question we have utilized the equations developed by K. C. Russell[12] and Russell and Powell[13] for the homogeneous nucleation of voids and vacancy loops. These equations are shown below:

$$J_k = Z' \beta_k N \exp(-\Delta G_k'/kT) \tag{15}$$

Z' = Zeldovich factor
β_k = capture rate
$\Delta G_k'$ = nucleation energy for critical nucleus

$$\Delta G_n' = \sum_{o}^{n-1} \ell n \left[\frac{\beta_i}{\beta_v} + \exp \frac{\delta G_n^\circ}{kT} \right] \tag{16}$$

$$\delta G_n' = \Delta G_{n+1}' - \Delta G_n^\circ \tag{17}$$

Voids

$$\Delta G_n^\circ = -nkT \ell n(N/N_v^e) + (4\pi)^{1/3} (3V)^{2/3} N^{2/3} \sigma \tag{18}$$

V = atomic volume
σ = surface energy

Loops

$$\Delta G_n^\circ = -nkT \ell n(N_v/N_v^e) + \frac{E_F}{6} (3.0n + 3.43n^{1/2}) \tag{19}$$

E_F = vacancy formation energy

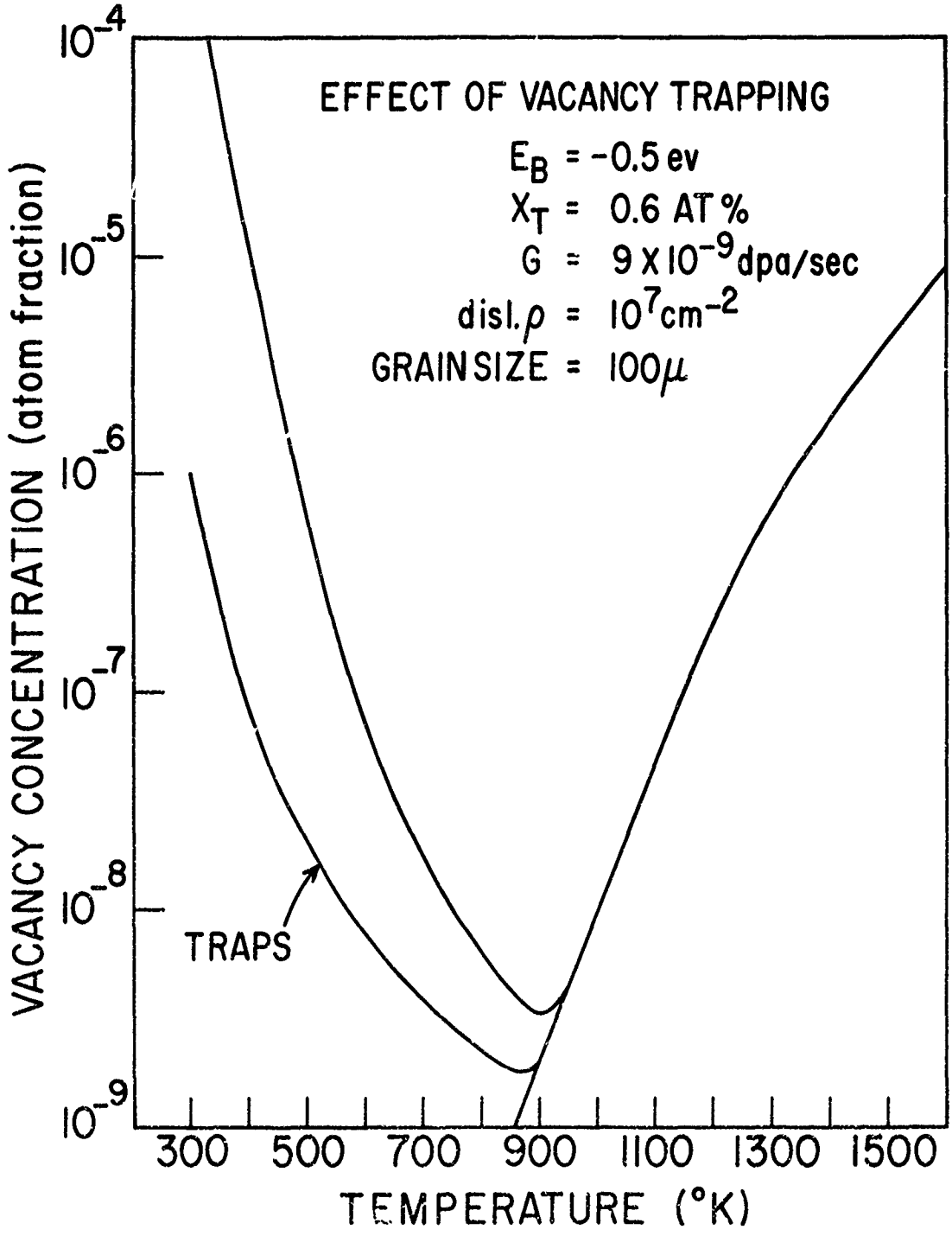

Fig. 11 - The effect of vacancy trapping on steady state vacancy concentration

Equation 15 is the basic nucleation equation in which the rate of nucleation, J, is given by the product of the capture rate, the Zeldovich factor, and the number of critical nuclei which are present. The $\Delta G_k'$ factor is a pseudo thermodynamic activation energy which includes a kinetic expression to account for the impingement of interstitials on the growing void nucleus, the β_i/β_v term in Eq. 16. $\Delta G_k'$ is the maximum value of $\Delta G_n'$ calculated in Eq. 16. The usual thermodynamic contributions for voids and loops are given in Eqs. 18 and 19 and the change as a function of n is given in Eq. 17. In practice one sums the values so calculated until a maximum in $\Delta G_n'$ is reached. This maximum represents the critical nucleus size and the height of the pseudo-free energy barrier gives the nucleation energy, $\Delta G_k'$. The model used for calculating the vacancy loop nucleation perhaps deserves some additional comment since it is based on a vacancy platelet model rather than on a dislocation loop model. This model for the vacancy loop nucleus gives much more realistic energies than does the model based on the strain energy of a dislocation loop[13]. The form shown in Eq. 19 is strictly applicable only to face centered cubic (fcc) metals, but we have used it as a first approximation for the present case since we are primarily looking for trends produced by vacancy trapping.

Calculations of void nucleation parameters are shown in Table 5. The cases of traps and no-traps refer to calculations made using the vacancy supersaturations shown in Fig. 11. The column headed B refers to the ratio β_i/β_v. B = 0 is for no interstitials present and B = 1 would hold for equal rates of impingement for vacancies and interstitials. It is believed that the situation in fast reactors is around .99. $\Delta G_k'$ (in electron volts) is the activation barrier for nucleation, n' is the critical nucleus size, and J_k is the nucleation rate in nuclei/cm^3/second.

The first case considered is for defect production in a water reactor at 550°K assuming a surface energy of 1200 ergs/cm^2. It can be seen that the presence of traps increases the barrier for nucleation from 1.30 to 1.81 ev for B = .9, increases the nucleus size, and drastically reduces the nucleation rate from 10^{12} to 10^4 per second.

The next set of data shows that the nucleation rate is extremely sensitive to the surface energy used in the calculations. A value as high as 1950 ergs/cm^2 has at times been suggested for iron but, as can be seen from the calculations, would essentially stop void nucleation.

Table 6 shows similar calculations for the nucleation of vacancy loops. These results were found to be extremely sensitive to the presence of traps and impingement rate for

Table 5

VOID NUCLEATION

Parameters	B	No Traps			Traps		
		ΔG_k	n'	J_k	ΔG_k	n'	J_k
Water Reactor	0	1.27	3	-	1.76	5	-
550°K	.9	1.30	4	1.1×10^{12}	1.81	8	7.1×10^{4}
1200 erg/cm²	.99	1.31	7	3.9×10^{11}	1.83	13	-
	0	5.45	12	-	7.55	20	-
1950 erg/cm²	.9	5.58	18	3.5×10^{-16}	7.78	32	-
	.99	5.61	29	-	7.85	57	-

Table 6

LOOP NUCLEATION

Parameters	B	No Traps		Traps	
		$\Delta G'_k$	n'	$\Delta G'_k$	n'
Water Reactor	0	.95	5	3.62	77
550°K	.9	1.17	35	>6.0	>100
1.4 ev	.99	>1.46	>100	-	-
	E_F				
Water Reactor	1.0	.21	1		
B = .9	1.3	.71	10		
550°K	1.4	1.16	35		
	1.5	>2.38	>100		

> Termination of $\Delta G'_n$ calculation at 100 steps.

interstitials. Although it appears that nucleation might occur if the bias factor were only .9 without considering traps, it appears extremely unlikely that homogeneous nucleation of vacancy loops would occur if traps were present. The activation energy and critical nucleus size are also extremely sensitive to the formation energy of the vacancy E_F. Vacancy formation energies in iron are believed to be 1.5 to 1.6 ev but, as noted previously, a bond model for fcc metals was used in these calculations so it is not surprising that more reasonable results are obtained with lower E_F.

The preceding calculations show quite clearly that the presence of vacancy traps with binding energy near .5 ev will depress void and vacancy loop nucleation rates in irradiated iron. We believe the vacancy trapping mechanism provides a satisfactory explanation of the absence of voids in the Fe-.3V alloy and also indicates that the enhanced nucleation of dislocation loops observed in the Fe-.3Cu alloy cannot be the result of a homogeneous nucleation mechanism. We must therefore examine more closely the case of nucleation on clusters of copper atoms or consider an unusually large binding energy in the copper system to explain the enhanced nucleation in that system.

There is some evidence to support a large binding energy between vacancies and copper atoms in iron in the form of tracer diffusion studies[14]. These results show a deviation of the Arrhenius plots of D vs 1/T indicative of more rapid diffusion of copper with a lower activation energy, an indication of a vacancy-copper interaction. The data are over a limited range, however, and are perturbed by the magnetic transformation of iron so that it is difficult to establish the magnitude of this binding energy.

The important conclusion of this study is that vacancy trapping even with relatively low binding energies is an effective method of reducing the vacancy supersaturation and hence the rate of void nucleation. A further bonus is that the interstitial concentration is also decreased. Although Russell has found the interstitial loop nucleation rate is only slightly influenced by such small changes in supersaturation, the decrease in interstitial concentration should slow the growth rate of interstitial loops. Future investigations of the utility of this approach will employ ion damage investigations of systems of interest.

III. CURRENT REACTOR PRESSURE VESSEL STEELS

A. Pressure Vessel Surveillance of the MH-1A Reactor

C. Z. Serpan, Jr.

The neutron-induced changes in the notch ductility and tension test characteristics of the Army MH-1A barge-mounted nuclear power reactor pressure vessel are being monitored by an in-reactor material surveillance program[15]. Capsules containing Charpy-V (C_V) and tension test specimens of the 3-1/4-in. AISI 316 SS vessel ring forging are located in both accelerated and near-vessel wall positions. In addition, neutron flux detector wires are positioned directly against the vessel wall to help eliminate some of the error associated with extrapolation of surveillance capsule data to the vessel wall.

A second accelerated-location surveillance capsule and vessel-wall location flux monitor have now been removed to continue the initial evaluation[16] of the MH-1A reactor vessel. These were both replacements and hence record the reactor operations for the period between 25 November 1969 and 19 May 1971. During this time the reactor operated a total of 8790 hours, at an average power level of 37.85 MW(t). Both the Charpy and tensile specimens were exposed to the reactor coolant during the irradiation. To preclude any possible crevice corrosion effects in the Charpy specimens, they were not notched during fabrication. Rather, they were notched in the hot cell following irradiation. Neutron flux detector wires were enclosed in a welded stainless steel tube during irradiation.

The results of evaluating the notched, Charpy specimens from the second MH-1A accelerated surveillance capsule are shown in Fig. 12. The three curves result from the fluence gradient across the capsule; no preirradiation condition curve is shown because energy absorption exceeds the testing machine capacity even at lowest attainable temperatures. It should be noted that the energy scale begins at 80 ft-lb rather than at 0 ft-lb. The uppermost curve shows test points at 200 and 300°F (93 and 149°C) which both exceeded the capacity of the test machine (205 ft-lb). The lower two curves both indicate a slight decrease in the upper energy shelf absorption capacity of the steel. A comparison of the present results to the previous surveillance data from the steel[16] indicate very close correspondence. The energy shelf decrease appears to be very nearly the same (150 to 170 ft-lb) for a fluence in the range of 1.0 to 1.5×10^{20} n/cm^2 >1 MeV.

The tension test data are summarized in Table 7. The specimens were taken from two different thickness locations

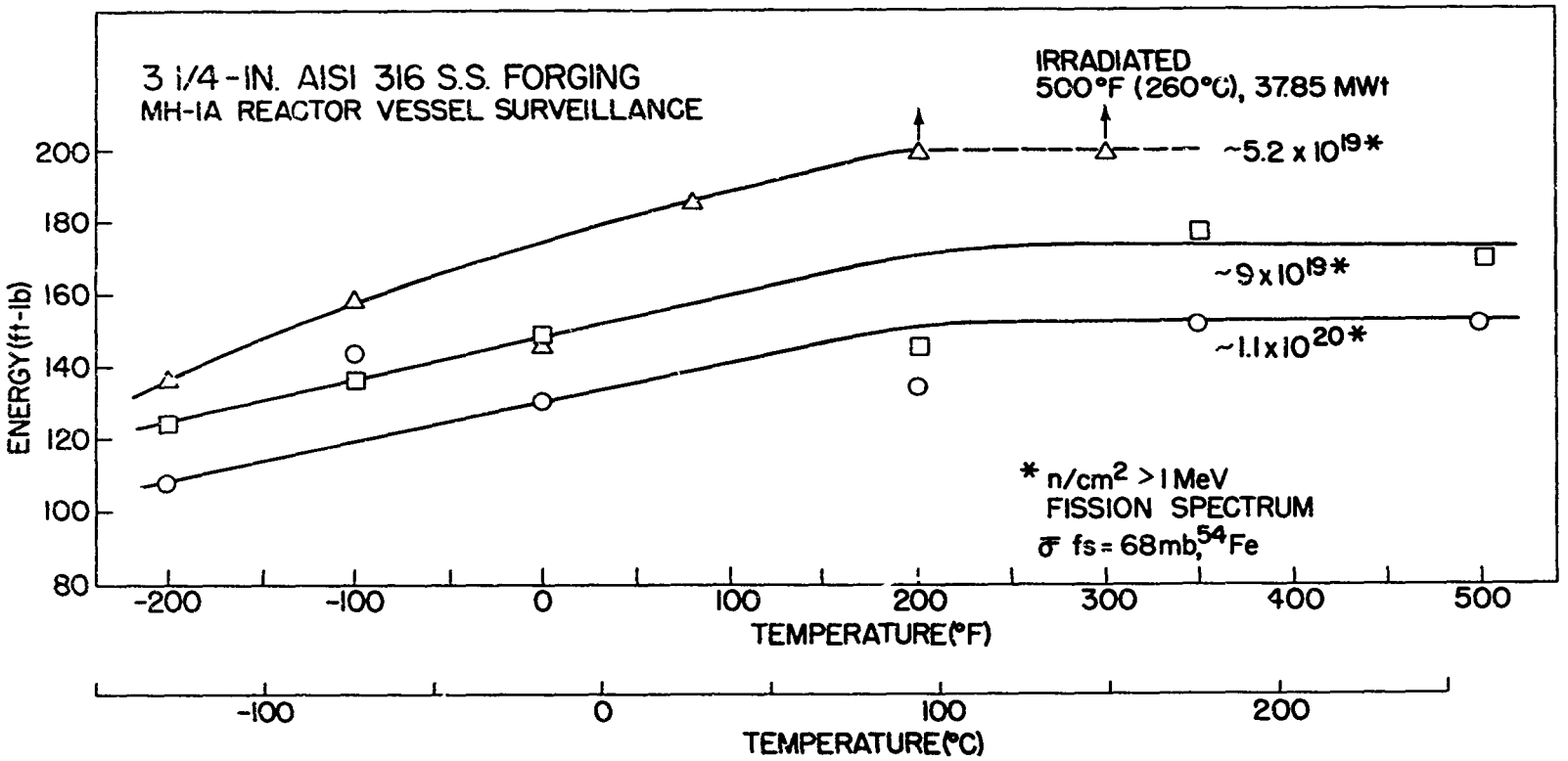

Fig. 12 - Charpy-V notch ductility characteristics of the 3-1/4-in. thick 316 stainless steel ring forging steel of the Army MH-1A reactor pressure vessel. Preirradiation condition, not shown, exceeds 205 ft-lb at all temperatures. Top curve indicates the steel exceeds test

Table 7

Tension Test Properties of 3-1/4-in. AISI 316 Stainless Steel Ring Forging of the MH-1A Pressure Vessel (500°F, 260°C)

Specimen No.	Neutron Fluence n/cm^2 >1 MeV*	0.2% Yield Strength Kpsi	Tension Strength Kpsi	Elongation %	Redn. in Area %
-	0	29.2	65.7	-	68.8
24	7×10^{19}	46.9	73.0	40.4	16.5
69	7×10^{19}	47.3	71.8	40.2	14.2
-	0	28.2	64.8	-	70.9
10	1.1×10^{20}	54.7	76.6	-	13.3
14	1.1×10^{20}	56.7	77.8	37.1	13.2

*Fission spectrum; $\tilde{\sigma}^{fs}$ = 68 mb, $^{54}Fe(n,p)^{54}Mn$.

in the MH-1A ring forging, hence the slight differences in recorded preirradiation properties. It should be noted that the yield strength has increased very much more than the tensile strength as a result of the irradiation. Furthermore, the amount of reduction in area has been significantly reduced by the irradiation. Note that the preirradiation, reduction in area values are both near 70%, but that following irradiation are about 13 to 15%. This degradation of reduction in area would appear to be closely related to the yield strength increase. A positive comparison with elongation values cannot be made because no preirradiation values were taken. However, it is well known that elongation in unirradiated 316 SS is very great at 500°F (260°C) so that the postirradiation values of near 40% while still reflecting high ductility suggest an appreciable reduction in this property.

Analysis of the neutron flux detector wires located in the vessel wall flux monitor are depicted and summarized in Fig. 13. The schematic representation indicates the location of the fuel core centerline and circumferential vessel weld with respect to the flux gradient along the vessel wall. It should be noted that the flux level at the weld is about 85% of the peak flux. This is of high interest because of the severe degradation observed in 316 SS weld deposits following irradiation as reported elsewhere[17].

Based upon the measured fluxes from this second operating period, fluences were calculated for a 20-year full power operating period for the MH-1A reactor. These are listed on Fig. 13 as 6.9×10^{19} n/cm^2 >1 MeV for the peak flux plane and 5.5×10^{19} n/cm^2 >1 MeV for the vessel weld. These values are somewhat lower than those estimated from the initial surveillance evaluations and may be more accurate because of the relatively steady, high power operations for this exposure period as opposed to the lower power, discontinuous operations for the initial operating period.

Replacement capsules have been fabricated and are undergoing irradiation in the accelerated locations of the MH-1A reactor. These contain newer types of specimens including resonance fatigue and compact tension. The most recent capsules prepared for insertion includes Charpy and tensile specimens of a submerged arc weld of 316 SS to evaluate the accelerated irradiation characteristics of this weld in the MH-1A spectrum. The high fluence to be attained by the MH-1A weld, plus the potential for 316 weld degradation, makes this an important new facet of the MH-1A surveillance program.

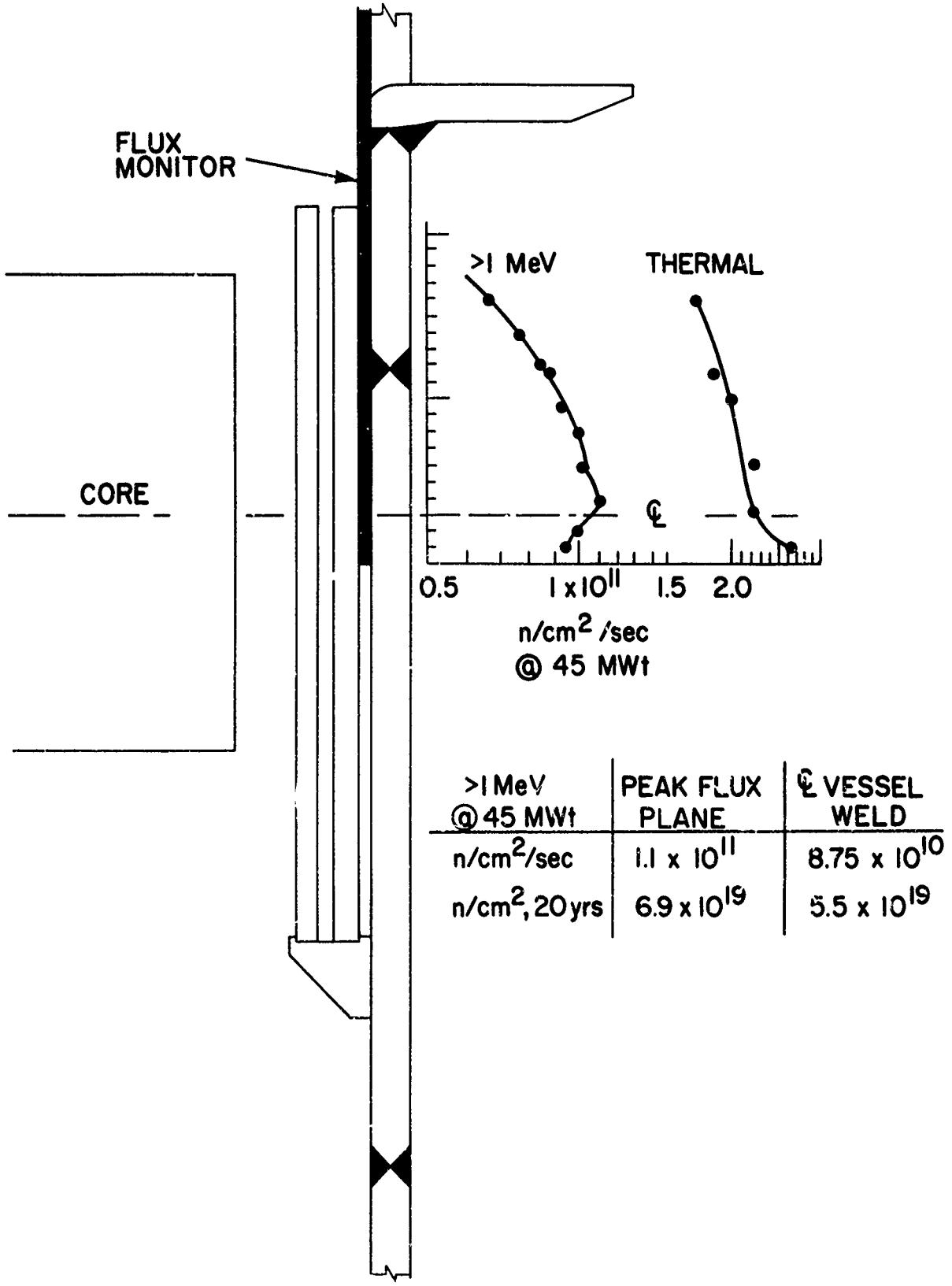

>1 MeV @ 45 MWt	PEAK FLUX PLANE	℄ VESSEL WELD
$n/cm^2/sec$	1.1×10^{11}	8.75×10^{10}
n/cm^2, 20 yrs	6.9×10^{19}	5.5×10^{19}

Fig. 13 - Neutron flux measurements along the pressure vessel wall of the Army MH-1A reactor. Flux values and 20-year fluences for the peak flux plane and for the circumferential vessel weld are tabulated.

REFERENCES

[1] F. J. Loss and R. A. Gray, Jr., "Fracture Toughness Characterization of Irradiated Stainless Steels," in Irradiation Effects on Reactor Structural Materials, QPR, 1 May-31 July 1972 (L. E. Steele, Editor), NRL Memorandum Report 2505, August 15, 1972, 28-48.

[2] G. E. Dieter, Jr., Mechanical Metallurgy, McGraw-Hill Book Co., Inc., New York, 1961, 249.

[3] J. M. Krafft et al, "Fracture-Flow Relationships for A533-B Pressure Vessel Steel," Trans. ASME, J. Eng. for Ind., Vol. 92, Series B, No. 2, May 1970, 330-338.

[4] R. J. Goode, "Identification of Fracture Plane Orientation," Materials Research and Standards, Vol. 12, No. 9, September 1972, 31.

[5] J. R. Hawthorne, "Demonstration of Improved Radiation Embrittlement Resistance of A533-B Steel Through Control of Selected Residual Elements," NRL Report 7121, May 29, 1970; and ASTM STP 484, 1971, 96-126.

[6] J. R. Hawthorne et al," Irradiation Effects on Reactor Structural Materials, QPR, 1 Nov 1966-31 Jan 1967," NRL Memorandum Report 1753, February 15, 1967; and Battelle-Northwest Report, BNWL-CC-1053, 1967.

[7] F. A Smidt, Jr., and H. E. Watson, "Effect of Residual Elements on Radiation Strengthening in Iron Alloys, Pressure Vessel Steels, and Welds," Metallurgical Trans., Vol. 3, August 1972, 2065-2073.

[8] F. A. Smidt, Jr. and J. A. Sprague, "Solute Effects on Defect Microstructure in Irradiated Iron," Trans. ANS, Vol. 15, No.1, June 1972, 244.

[9] A. C. Damask and G. J. Dienes, Point Defects in Metals, Gordon and Breach, New York, 1963.

[10] H. W. Wiedersich, in Vol. II, Proceedings of International Conference on the Strength of Metals and Alloys, ASM, Metals Park, Ohio, 1970, 784.

[11] S. D. Harkness and C. Li, "A Study of Void Formation in Fast Neutron-Irradiated Metals," Metallurgical Trans., Vol. 2, 1971, 1457.

(Page 46 is blank)

[12] K. C. Russell, "Nucleation of Voids in Irradiated Metals," Acta Met., Vol. 19, 1971, 753.

[13] K. C. Russell and R. W. Powell, "Dislocation Loop Nucleation in Irradiated Metals," to be published in 1972.

[14] V. Irmer and M. Feller-Kniepmeier, "On the Influence of Impurity Atoms on Shelf Diffusion in α-iron Single Crystals," Phil. Mag., Vol. 25, 1972, 1345.

[15] C. Z. Serpan, Jr. and H. E. Watson, "Pressure-Vessel Surveillance Program for the Army MH-1A Floating Nuclear Power Reactor," NRL Report 6604, September 22, 1967.

[16] L. E. Steele et al, "Irradiation Effects on Reactor Structural Materials, QPR, 1 Aug-31 Oct 1970," NRL Memorandum Report 2181, November 15, 1970; and WHAN-FR-401, January 1971.